quantum reports

MDPI

Article

Operational Causality Without Definite Order: Certifying Indefinite Causal Structure via a Causal Inequality and Causal Witness

Horace T. Crogman

Department of Physics, California State University, Dominguez Hills, Carson, CA 90747, USA; hcrogman@csudh.edu

Abstract

Quantum processes with indefinite causal order challenge the classical assumption that operations must occur in a single fixed temporal sequence. The quantum switch provides a concrete setting in which two operation orders, $A \prec B$ and $B \prec A$, are coherently controlled by a quantum system. In the strict process matrix formulation of the lazy guess your neighbour's input (LGYNI) game, however, quantum theory, including the quantum switch, does not violate the standard causal inequality when probabilities are computed solely from local instruments. In this work, we study an extended control-assisted operational protocol in which the control system of the quantum switch is measured and used to define the task output. We compare increasingly expressive strategy classes, including single-qubit SU(2) operations, product target-ancilla operations, and entangling Cartan-decomposed two-qubit operations with generalized POVMs. Restricted models saturate or remain below the 3/4 fixed-order benchmark, whereas the optimized Cartan + ancilla + POVM strategy reaches $P_{\mathrm{succ}}^{\mathrm{ext}} \approx 0.83596$, demonstrating enhanced task performance within the extended protocol. The optimized strategy remains operationally no-signaling to numerical precision and retains its extended protocol advantage under more than 25% white noise admixture. These results identify the operational resources required for control-assisted quantum switch enhancement and support the view that indefinite temporal order can be used as a quantum informational resource without implying a breakdown of operational causality.

Keywords: indefinite causal order; process matrices; quantum switch; causal inequality; causal witness; quantum information theory; semidefinite programming; quantum resources

Check for updates

Academic Editors: Mingxing Luo, Ming Li and Xue Yang

Received: 24 April 2026
Revised: 29 May 2026
Accepted: 1 June 2026
Published: 3 June 2026

Copyright: © 2026 by the author. Licensee MDPI, Basel, Switzerland. This article is an open access article distributed under the terms and conditions of the Creative Commons Attribution (CC BY) license.

1. Introduction

In ordinary quantum circuits, operations are arranged in a definite order. A gate A is applied before a gate B, or B is applied before A. The quantum switch changes this picture by allowing the order itself to be controlled by a quantum system. If the control qubit is in state $|\,0\rangle$, the target system experiences one order, for example, $A \prec B$. If the control qubit is in state $|\,1\rangle$, the target experiences the reverse order, $B \prec A$. When the control is prepared in a coherent superposition, the two possible orders can interfere. This is the sense in which the quantum switch realizes coherent control of causal order.

This is not the same as a classical random switch. In a classical random switch, a bit selects either $A \prec B$ or $B \prec A$ in each run. The observer may not know which order occurred, but the order is still definite in that run. In the quantum switch, the

two alternatives are not merely selected at random; they remain phase coherent. The question is whether this coherence between orders can be used as a physical resource while still preserving operational causality.

The process matrix framework introduced by Oreshkov, Costa, and Brukner provides a natural setting for this question [1]. In that framework, local quantum operations can be embedded in a larger process without assuming a predefined global causal order. A process is causally separable if it can be written as a fixed order $A \prec B$, a fixed order $B \prec A$, or a convex mixture of the two. Such a mixture represents classical uncertainty about the order. A causally non-separable process, in contrast, cannot be reduced to any such mixture.

The quantum switch, introduced as a higher-order transformation of quantum operations [2], is the standard example of indefinite causal order. Subsequent work showed that the quantum switch is causally non-separable and that this non-separability can be certified using causal witnesses, thereby distinguishing indefinite causal order from classical mixtures of fixed causal orders [3]. It has been studied theoretically and implemented experimentally in photonic and related platforms [4–7]. These experiments show that indefinite order is not merely a formal construction: one degree of freedom can coherently control the order in which operations act on another. Indefinite causal order has also been shown to provide information processing advantages, including improved communication through noisy channels and reductions in communication complexity [8–14].

At the same time, the role of the quantum switch in causal games is subtle. In the standard lazy guess your neighbor's input (LGYNI) causal inequality, quantum theory does not violate the causal bound when probabilities are computed solely from local instruments [13]. This includes the quantum switch when the future control system is not used as part of the task output. Araújo et al. showed that the quantum switch is causally non-separable and can be detected by a causal witness, but causal non-separability and causal inequality violation are not the same notion [3].

More recently, van der Lugt, Barrett, and Chiribella showed that device-independent certification of indefinite causal order is possible for the quantum switch when the scenario is enlarged to include an additional spacelike separated observer and Bell-type constraints [15]. This result is important because it separates two questions. One question is whether indefinite causal order can be certified device-independently in enriched scenarios. A different question is whether measurement access to the control system can improve task performance in a specific operational protocol. The present paper addresses the second question.

We therefore do not claim a device-independent violation of the standard LGYNI causal inequality. Instead, we study an extended control-assisted protocol in which the control system of the quantum switch is measured after the switch operation and used to define the task output. The corresponding success probability is denoted as $P_{\mathrm{succ}}^{\mathrm{ext}}$. A value above ¾ is interpreted here as enhanced task performance relative to the fixed-order benchmark within this extended protocol, not as a strict violation of the standard LGYNI inequality.

This distinction also clarifies what is meant by causal consistency in the present work. Causal consistency does not mean that the global temporal order is definite. Rather, it means that the observed input–output statistics remain operationally no-signaling. Party A's marginal statistics should not reveal party B's input, and party B's marginal statistics should not reveal party A's input. In this sense, temporal order may be indefinite while the observable statistics still avoid superluminal signaling, retrocausal signaling, or causal-loop behavior.

The random elements of the protocol are also specific. The inputs x and y, together with the task bit b', are sampled uniformly as classical random variables. The measurement

outcome is quantum-random in the usual Born-rule sense. The order of operations, however, is not chosen by a hidden classical random variable. It is coherently controlled by the control qubit. A classical random variable produces a mixture of orders; a coherent control qubit allows for interference between the two alternatives.

The central question of this paper is therefore as follows:

Which operational resources are needed for a quantum switch protocol to exceed the fixed-order task benchmark while preserving operational no-signaling?

To answer this question, we compare three increasingly expressive model families. The first uses single-qubit SU(2) operations without an ancilla. The second adds a target–ancilla but restricts the local operations to product two-qubit channels. The third uses fully entangling Cartan-decomposed two-qubit operations together with task-dependent positive operator-valued measures (POVMs) on the control system. All three models are evaluated using the same success probability objective and optimization framework.

The resulting hierarchy is clear. Restricted SU(2) strategies and product ancilla strategies saturate or remain below the fixed-order benchmark. Enhanced performance appears only when the strategy includes entangling target–ancilla dynamics and generalized control measurements. In the optimized Cartan + ancilla + POVM model, we obtain $P_{\mathrm{succ}}^{\mathrm{ext}} \approx 0.83596$, while the operational no-signaling deviations remain at numerical precision. The advantage also persists under more than 25% white noise admixture.

The physical message is that indefinite causal order does not mean that causality disappears. Rather, temporal order can become a coherent quantum degree of freedom. When that degree of freedom is preserved and measured in the appropriate operational setting, it can improve task performance. At the same time, the observed statistics can remain causally consistent.

Our aim is more specific than proving a new device-independent causal inequality violation. We use the quantum switch as a test case and ask which ingredients are needed to improve the task score once the control system is available for readout. The simulations point to a clear answer: the advantage appears only when entangling target–ancilla dynamics and flexible control measurements are included. In this way, this work treats indefinite causal order as a quantum informational resource rather than a breakdown of causality.

2. Materials and Methods

Throughout this work, the background higher-order process is the quantum switch. The optimization does not vary the higher-order process itself; rather, it varies the local operations and measurements applied within a fixed quantum switch architecture. This section defines the operational task, distinguishes the standard LGYNI/process matrix setting from the extended control-assisted protocol used here, describes the simulation families, and explains the optimization, noise, witness, and no-signaling procedures.

2.1. Operational Task and Meaning of Causal Consistency

We consider the lazy guess your neighbor's input (LGYNI) causal game [3,13], also referred to here as the random task causal game because a task bit b' determines which party must guess the other party's input. In the standard process matrix formulation, two parties, A and B, receive classical inputs $x, y \in \{0,1\}$ and produce outputs $a, b \in \{0,1\}$ through local instruments $M_{a|x}$ and $N_{b|y}$. The joint probabilities are given by the generalized Born rule,

$$p(a,b \mid x,y) = \mathrm{Tr}\Big[\Big(M_{a|x} \otimes N_{b|y}\Big) W\Big]. \tag{1}$$

where W is the process matrix.

For all causally separable processes, namely, fixed order $A \prec B$, fixed order $B \prec A$, or convex mixtures of these two orders, the standard LGYNI success probability satisfies

$$P_{\text{succ}} \leq \frac{3}{4}. \tag{2}$$

It is known that quantum theory, including the quantum switch, does not violate the standard LGYNI causal inequality when probabilities are computed solely from local instruments and the future control system is not used as part of the output [13]. Therefore, the present work should not be interpreted as a device-independent violation of the standard LGYNI causal inequality.

Instead, we study an extended control-assisted operational protocol. In this protocol, the control system of the quantum switch is measured after the switch operation, and the control measurement outcome is used to define the task output. The corresponding success probability is denoted as

$$P_{\text{succ}}^{\text{ext}}(\theta), \tag{3}$$

where θ is the parameter vector specifying the local operations and measurements.

In this paper, "causal consistency" means operational no-signaling at the level of the observed statistics. It does not mean that the global temporal order is definite. Thus, the protocol may coherently superpose $A \prec B$ and $B \prec A$, but the measured marginal statistics must not allow party A to infer y, nor party B to infer x, outside of the allowed task structure. This is the sense in which the protocol can have indefinite order while preserving operational causality.

2.2. Random Variables and Coherent Control of Order

The classical random variables in the protocol are the inputs x, y, and the task bit b', all sampled uniformly from $\{0,1\}$. The task rule is simple: when $b' = 0$, party A must guess y; when $b' = 1$, party B must guess x. Measurement outcomes are quantum random in the usual Born-rule sense.

The order of operations, however, is not selected by a classical random variable. It is controlled coherently by the control qubit of the quantum switch. This distinction is central. A classical random switch gives a mixture of definite orders. A quantum switch preserves coherence between the two alternatives, allowing interference between the histories $A \prec B$ and $B \prec A$.

With uniformly sampled inputs and task bit, the extended success probability is

$$P_{\text{succ}}^{\text{ext}}(\theta) = \frac{1}{8}\sum\nolimits_{x,y\in\{0,1\}} \left[p\left(a = y \mid x, y, b' = 0, \theta\right) + p\left(b = x \mid x, y, b' = 1, \theta\right)\right]. \tag{4}$$

A value $P_{\text{succ}}^{\text{ext}} > 3/4$ is interpreted as enhanced task performance relative to the fixed-order benchmark within the extended control-assisted protocol. It is not, by itself, a strict device-independent violation of the standard LGYNI causal inequality.

2.3. Quantum Switch Implementation

The quantum switch coherently controls the order in which two input-dependent operations $U_A(x)$ and $U_B(y)$ act on a target system. The control qubit is initialized in $|+\rangle_c = (|0\rangle_c + |1\rangle_c)/\sqrt{2}$. The target is initialized in $|0\rangle_t$, and when an ancilla is present it is initialized in $|0\rangle_a$.

For each input pair (x, y), the switch unitary is

$$U_{\text{switch}}(x,y) = |0\rangle\langle 0|_c \otimes U_B(y)U_A(x) + |1\rangle\langle 1|_c \otimes U_A(x)U_B(y). \tag{5}$$

The output state is

$$|\psi_{\text{out}}(x,y)\rangle = U_{\text{switch}}(x,y)\,|\psi_{\text{in}}\rangle. \tag{6}$$

This circuit-level representation is used in all simulations. It provides a direct implementation of coherent order control and makes clear how the two possible operation orders can interfere before the final measurement.

2.4. Control-Based Outcome Definition

In the standard process matrix LGYNI setting, outputs are generated exclusively by local instruments. In the present extended protocol, the output is defined by measuring the control qubit after the switch operation (see Figure 1).

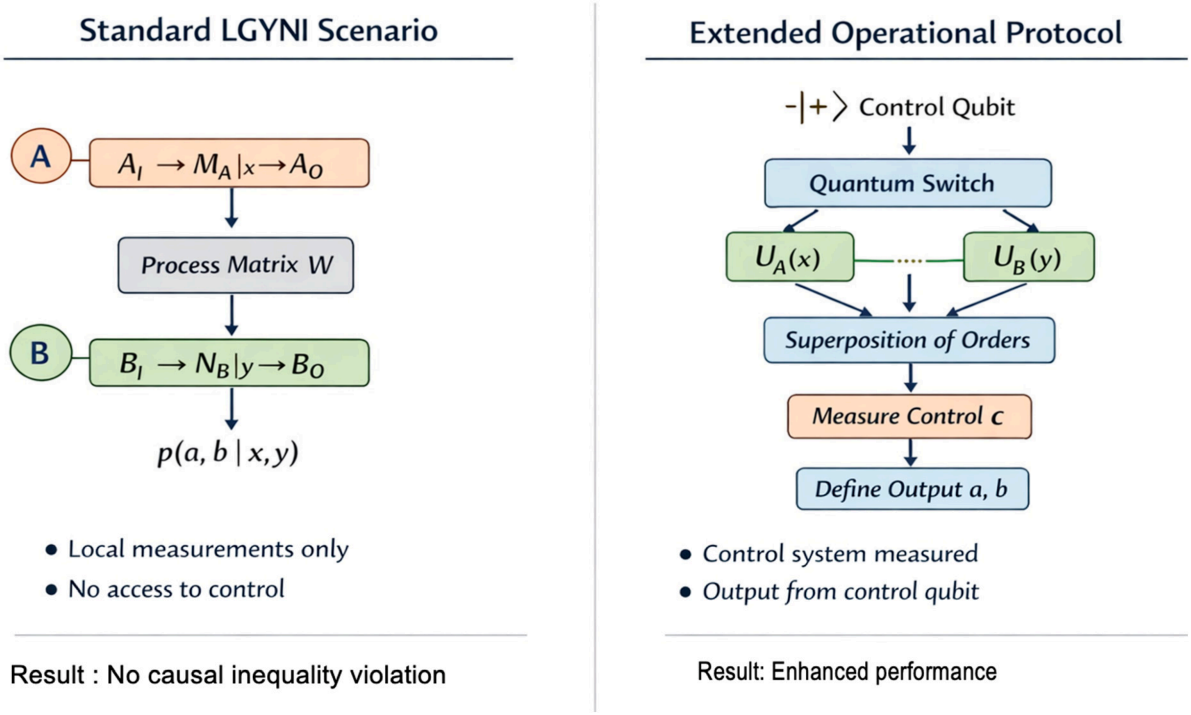


Figure 1. Comparison between the standard process-matrix LGYNI scenario and the extended operational protocol considered in this work. Here, A and B denote the two parties/laboratories in the causal game: A receives input x and B receives input y. In the standard formulation (**left**), outcomes are generated solely by local instruments, and the quantum switch reduces to a convex mixture of fixed causal orders, preventing violation of the causal inequality. In the extended protocol (**right**), the control system is explicitly measured and used to define the output variable, leading to enhanced task performance while preserving operational no-signalling.

For $b' = 0$, the control measurement outcome is interpreted as A's guess of y. For $b' = 1$, the control measurement outcome is interpreted as B's guess of x. If $E^{(k)}_{b'}(\theta)$ denotes the k-th effect of the task-dependent control measurement, then the probabilities used in the task are

$$p(a = y \mid x, y, b' = 0, \theta) = \langle\psi_{\text{out}}(x,y)\mid \left(E^{(y)}_0(\theta)\otimes \mathbb{I}_{t,a}\right)\mid \psi_{\text{out}}(x,y)\rangle. \tag{7}$$

and

$$p(b = x \mid x, y, b' = 1, \theta) = \langle\psi_{\text{out}}(x,y)\mid \left(E^{(x)}_1(\theta)\otimes \mathbb{I}_{t,a}\right)\mid \psi_{\text{out}}(x,y)\rangle. \tag{8}$$

The detailed basis states and POVM parameterization are given in Appendix A.

This distinction is essential: the protocol studied here is an extended measurement scenario, not the strict standard LGYNI scenario.

2.5. Simulation Families and Resource Hierarchy

We compare three increasingly expressive simulation families. This hierarchy is designed to determine which operational resources are necessary for enhanced performance in the extended protocol.

First, we consider single-qubit SU(2) channels without ancilla. In this model, each party applies an input-dependent single-qubit unitary to the target. Each unitary is parameterized by a ZYZ Euler decomposition,

$$U(\alpha, \beta, \gamma) = e^{-i\alpha Z/2} e^{-i\beta Y/2} e^{-i\gamma Z/2}. \tag{9}$$

The control measurement is projective and task-dependent. This model tests whether coherent control of order and projective control readout alone are sufficient to exceed the fixed-order benchmark.

Second, we consider product target–ancilla channels. A one-qubit ancilla is appended, but the parties' operations are restricted to product form on target $\otimes$ ancilla,

$$U_A(x) = U_A^{(t)}(x) \otimes U_A^{(a)}(x), U_B(y) = U_B^{(t)}(y) \otimes U_B^{(a)}(y). \tag{10}$$

This model tests whether ancilla assistance alone, without entangling target–ancilla dynamics, is sufficient for enhanced performance.

Third, we consider entangling Cartan two-qubit channels with control POVMs. Each party applies a general two-qubit unitary on target $\otimes$ ancilla using a Cartan/KAK decomposition,

$$U = (V_1 \otimes V_2) \exp\left[-\frac{i}{2}(\alpha X \otimes X + \beta Y \otimes Y + \gamma Z \otimes Z)\right](V_3 \otimes V_4). \tag{11}$$

Here, each V_j is a single-qubit SU(2) unitary, and α, β, γ are Cartan entangling angles. This gives 15 parameters per input-dependent two-qubit unitary, or 60 channel parameters across the two inputs for A and the two inputs for B.

In the most expressive model, the control measurement is also generalized to task-dependent two-outcome POVMs. The POVM construction enforces positivity and normalization during optimization. This adds eight measurement parameters, giving 68 real parameters in the full Cartan + POVM model. This model tests whether entangling target–ancilla operations and generalized control measurements are required to obtain the observed enhancement.

2.6. Success Probability Evaluation

For each candidate parameter vector θ, the simulation evaluates all eight branches defined by $x, y, b' \in \{0, 1\}$. The algorithm constructs $U_A(x)$ and $U_B(y)$, builds the switch unitary, evolves the input state, computes the task-dependent correct guess probabilities, and averages them according to Equation (4).

Numerical values of $P_{\text{succ}}^{\text{ext}}$ are clipped to $[0, 1]$ only to suppress floating point roundoff error. This clipping is not used to alter the optimization landscape.

The ideal control-assisted quantum switch construction can reach

$$P_{\text{succ}}^{\text{ext}} = \frac{1}{2}\left(1 + \frac{1}{\sqrt{2}}\right) = \frac{2 + \sqrt{2}}{4} \approx 0.8536. \tag{12}$$

This value is not a universal replacement for the standard LGYNI bound. It applies to an extended operational construction in which the control remains coherent and is available for task-dependent measurement. If the control is traced out, decohered, inaccessible, or excluded from the output definition, the standard process matrix limitation is recovered.

2.7. Optimization Pipeline

The optimization seeks

$$\theta^\star = \arg\max_\theta P_{\text{succ}}^{\text{ext}}(\theta). \tag{13}$$

or equivalently minimizes

$$f(\theta) = -P_{\text{succ}}^{\text{ext}}(\theta). \tag{14}$$

The search landscape is highly non-convex, particularly for the 68-parameter Cartan + POVM model. We therefore use a global–local–multi-start pipeline. The global stage uses differential evolution to explore the parameter space broadly. In higher-budget searches, a covariance matrix adaptation evolution strategy may also be used. The best global candidate is then refined using Nelder–Mead. Finally, additional local refinements are launched from small perturbations around the best candidate to reduce the chance of remaining in a shallow local basin.

All angle-like parameters are bounded to $[-\pi, \pi]$. After noisy perturbations, angles are wrapped back into this interval. The complete optimization structure is summarized as

$$\theta_{\text{global}} \to \theta_{\text{local}} \to \theta_{\text{final}}. \tag{15}$$

The full parameter construction, simulation, optimization, and optional witness-certification workflow is summarized in Figure 2.

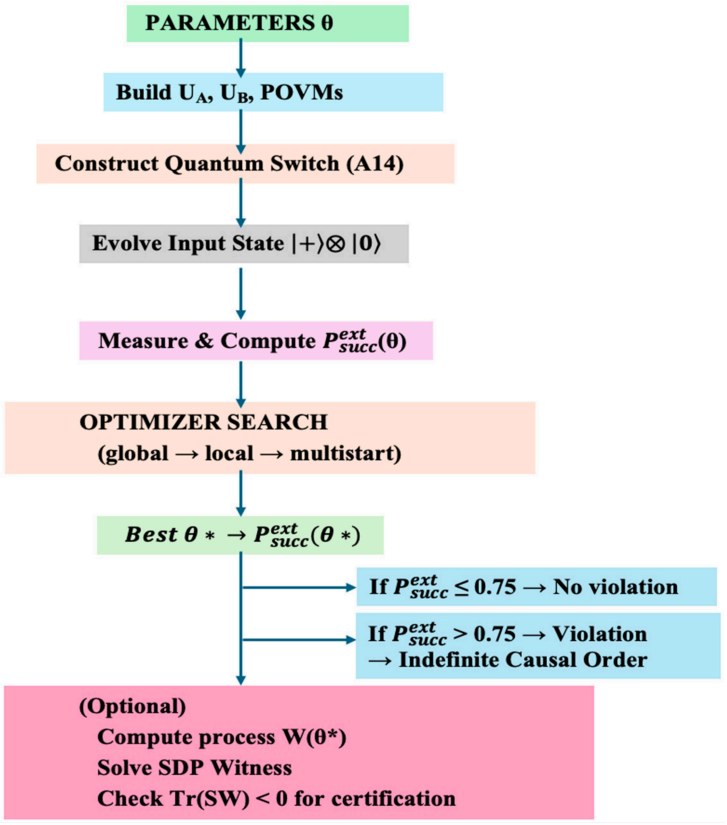


Figure 2. Workflow for parameter optimization, simulation, and optional certification of nonclassical causal structure in the extended operational protocol. Given a parameter vector θ, the protocol constructs the party operations U_A, U_B and task-dependent measurements, builds the quantum switch unitary, evolves the input state, evaluates $P_{\text{succ}}^{\text{ext}}(\theta)$, and maximizes it using a global–local–multi-start optimization pipeline. The optimized value is compared with the ¾ fixed-order benchmark. Optionally, the associated process matrix may be tested using a causal witness.

Additional step-by-step flow diagrams for the theoretical setup, parameterized strategy, causal-game evaluation, optimization pipeline, benchmark comparison, and optional causal-witness certification are provided in Appendix B, Figures A1–A6.

2.8. Noise Robustness Analysis

To quantify robustness, the optimized strategy is mixed with uniform white noise of strength p. Because a fully noisy strategy gives random guessing, the noisy success probability is modeled as

$$P_{\text{succ}}^{\text{ext}}(p) = (1-p)P_{\text{succ}}^{\text{ext}}(0) + p\left(\frac{1}{2}\right). \tag{16}$$

The critical noise value $p^\star$ is defined by $P_{\text{succ}}^{\text{ext}}(p^\star) = 3/4$. For the ideal quantum switch benchmark in Equation (12), this gives $p^\star = 2 - \sqrt{2}$. For the optimized numerical strategy, $p^\star$ is computed using the optimized value of $P_{\text{succ}}^{\text{ext}}(0)$, and the full curve is generated by sweeping p over $[0,1]$.

2.9. Operational No-Signaling Checks

Operational no-signaling is checked directly from the simulated observed statistics. The relevant conditions are

$$p(a \mid x, y, b') \text{ independent of } y,\ p(b \mid x, y, b') \text{ independent of } x. \tag{17}$$

The local marginals are computed from $p(a, b \mid x, y, b')$, and the maximum absolute deviations from the independence conditions are reported for each optimized parameter set. In an experimental implementation, the same quantities would be reported with statistical uncertainty. This no-signaling condition is specific to the implemented measurement protocol. It verifies that the observed input–output statistics do not permit operational signaling. It does not imply that the underlying process matrix is no-signaling in every possible operational context.

2.10. Causal Witness Certification

As a complementary device-dependent certification step, the optimized strategy may be associated with a process matrix estimate $W(\theta^\star)$. A causal witness is a Hermitian operator S satisfying

$$\text{Tr}\left(SW_{\text{sep}}\right) \geq 0 \text{ for all causally separable processes } W_{\text{sep}}, \tag{18}$$

A negative witness value certifies that the reconstructed or simulated process lies outside of the cone of causally separable processes.

The witness search is formulated as a semidefinite program over the dual cone of causally separable processes. The fixed-order cones $A \prec B$ and $B \prec A$ are imposed through linear constraints corresponding to no signaling from future to past for each definite order. A normalization condition is added to remove the trivial zero solution. The simulations were implemented in Python 3.11.2 using NumPy 1.24.0 and SciPy 1.14.1. The optional causal-witness semidefinite programs were written for CVXPY, with MOSEK used when available and SCS used for prototyping; because the witness pipeline is optional and was not used to generate the main numerical results, solver versions should be reported for any production SDP run.

This witness analysis is distinct from the extended protocol success probability analysis. The main numerical result is task enhancement in an extended control-assisted protocol.

The witness provides an additional device-dependent certification layer when process matrix reconstruction is available.

2.11. Experimental Implementation Considerations

The circuit-level model is compatible with existing quantum switch implementations in which a control degree of freedom coherently routes a target system through two alternative orders. In photonic platforms, the control may be encoded in path or polarization, while the target and ancilla may be encoded in additional photonic degrees of freedom. In circuit-based platforms, the same logical structure may be implemented using controlled routing, controlled SWAP operations, or equivalent decompositions into entangling gates.

The generalized POVMs used in the Cartan + POVM model may be implemented by coupling the control to an auxiliary system followed by projective measurement, as in standard dilation-based measurement constructions. Thus, the POVM should be interpreted as an effective measurement description, not as an unphysical operation.

The present work does not provide a full hardware compilation of the optimized Cartan parameters into a specific experimental gate set. Instead, it identifies the operational resources required for enhanced performance: coherence of the control system, controllable target–ancilla interactions, and flexible control-system measurement.

2.12. Software and Reproducibility

All simulations are implemented in Python/NumPy using explicit tensor products and state vector or density matrix updates. Each objective function evaluation averages over the eight input/task branches defined by x, y, and b'. For each run, the model class, parameter dimension, random seed, optimizer settings, restart count, best parameter vector, and best value of $P_{\text{succ}}^{\text{ext}}$ are recorded. Output files include parameter tables, optimizer traces, success probability plots, and noise robustness plots. The SDP-based causal witness routines are implemented separately in Python/CVXPY.

3. Results

3.1. Analytic Benchmark and Noise Robustness in the Extended Protocol

As a theoretical reference, we first analyze the performance of the quantum switch protocol within the extended operational model defined in Section 2. In the standard process matrix formulation of the LGYNI causal game, the success probability is bounded by Equation (2), and it is known that quantum processes, including the quantum switch, do not violate this bound when probabilities are computed solely from local instruments.

In contrast, in the present model, the success probability $P_{\text{succ}}^{\text{ext}}$ is defined through a control-assisted measurement protocol. In the ideal limit, suitable choices of local operations and control measurements yield the known quantum switch value

$$P_{\text{succ}}^{\text{ext}} = \frac{1}{2}\left(1 + \frac{1}{\sqrt{2}}\right) \approx 0.8536, \tag{19}$$

which exceeds the ¾ fixed-order benchmark within the extended protocol.

We emphasize that this value corresponds to the extended operational protocol, and not to the standard LGYNI causal inequality evaluated within the strict process-matrix framework.

To assess robustness, we introduce white noise according to the model defined in Section 2.6 and evaluate $P_{\text{succ}}^{\text{ext}}(p)$. As the noise parameter increases, the success probability decreases smoothly toward the random guess value ½. The resulting curve (Figure 3) shows that the (3/4) fixed-order benchmark is exceeded over a finite interval of noise strengths, demonstrating that the observed advantage is not restricted to an idealized point.

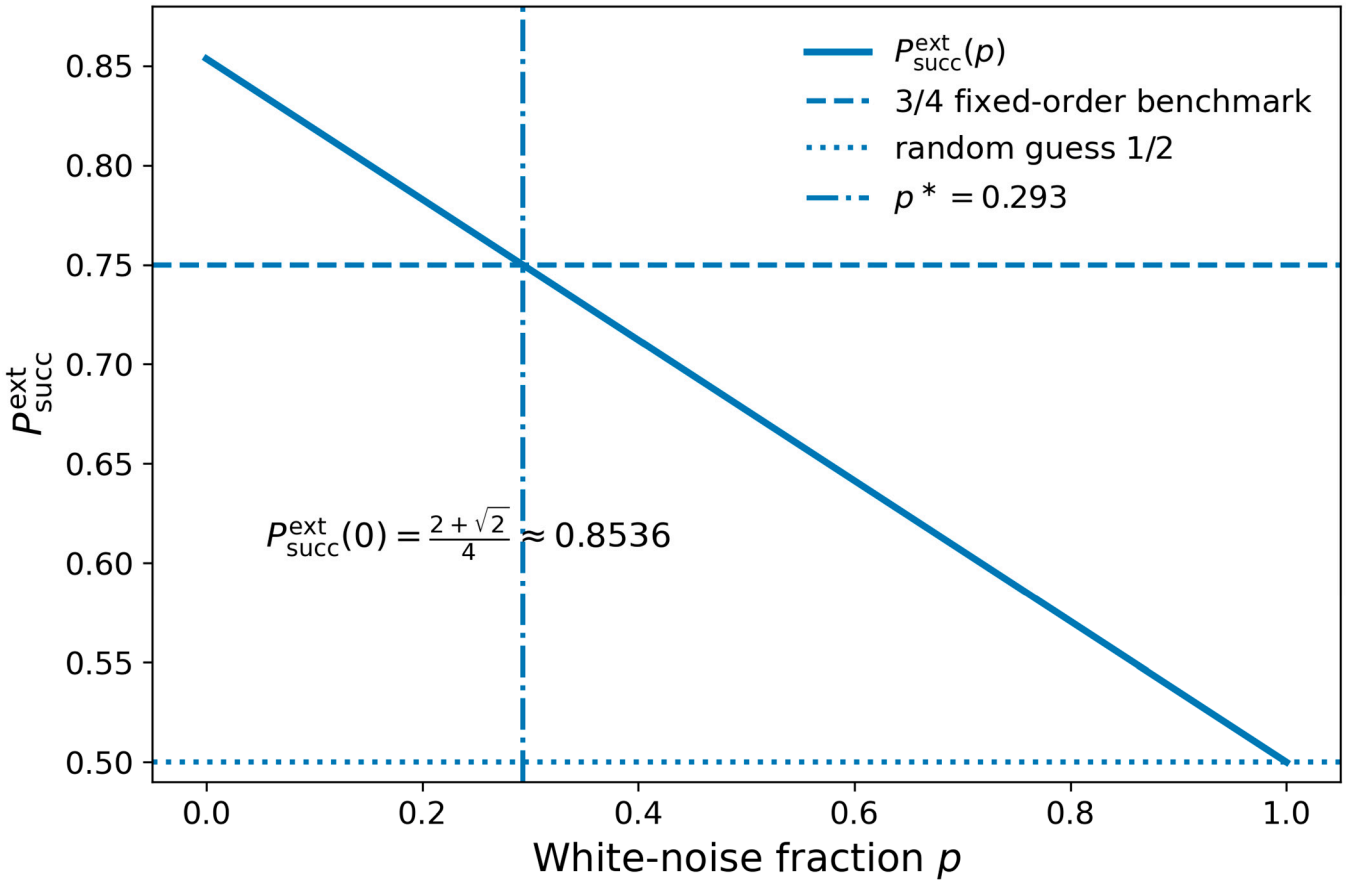


Figure 3. Analytic noise robustness of the ideal quantum switch in the extended operational protocol. The plot shows the extended success probability $P^{\text{ext}}_{\text{succ}}$ as a function of white-noise visibility p. At $p = 0$, the protocol attains the ideal value $P^{\text{ext}}_{\text{succ}} = \left(2+\sqrt{2}\right)/4 \approx 0.8536$, above the ¾ fixed-order benchmark; as noise increases, $P^{\text{ext}}_{\text{succ}}$ decreases smoothly toward the random-guess value 1/2. If shown, p^* denotes the critical noise value at which $P^{\text{ext}}_{\text{succ}}$ reaches the ¾ benchmark; the superscript $*$ labels this threshold and is not an independent variable. This figure corresponds to the extended operational model defined in Section 2, not to the standard LGYNI causal inequality evaluated within the strict process-matrix framework.

3.2. Numerical Emulation with Restricted Models

We next implement numerical simulations of the protocol using increasingly expressive classes of local operations.

(i) Single-qubit SU(2) channels (no ancilla)

In the simplest model, each party applies a single-qubit SU(2) unitary to the target system, and the control qubit is measured projectively. Optimization over the parameter vector θ is performed using the global–local pipeline described in Section 2.5.

The best value obtained is

$$P^{\text{ext}}_{\text{succ}} \approx 0.7497, \tag{20}$$

which is numerically indistinguishable from the ¾ fixed-order benchmark. Repeated optimization runs converge to values tightly clustered near this bound (Figure 4), indicating that this restricted model does not yield an advantage within the extended protocol.

(ii) Product two-qubit channels with ancilla

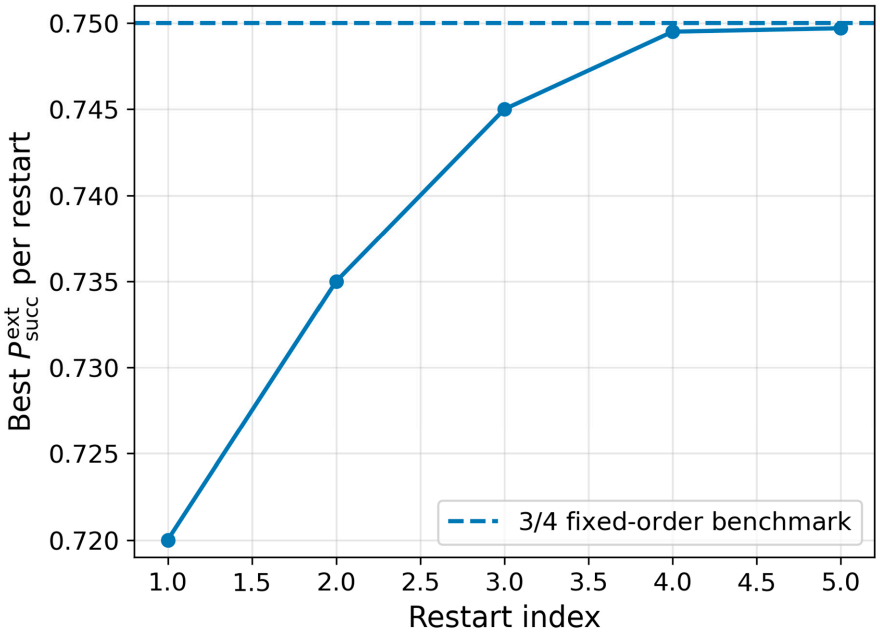


Figure 4. Optimizer performance for the quantum switch in the single-qubit SU(2) model without ancilla. Each point gives the best extended success probability $P_{\text{succ}}^{\text{ext}}$ obtained per restart during global-plus-local optimization over single-qubit SU(2) channels. The optimizer converges near $P_{\text{succ}}^{\text{ext}} \approx 0.7497$, consistent with the 3/4 fixed-order benchmark, indicating that this restricted model does not yield enhanced performance within the extended protocol. The solid line is included solely as a visual guide connecting the best success probability obtained in each restart and does not represent a dynamical trajectory, fit, or interpolation model.

We then extend the model by including a one-qubit ancilla while restricting local operations to product unitaries on target⊗ancilla. Under the same optimization procedure, we obtain

$$P_{\text{succ}}^{\text{ext}} \approx 0.7477, \tag{21}$$

which remains below the 3/4 fixed-order benchmark within the extended protocol. As shown in Figure 5, the optimizer consistently converges near this value, indicating that separable ancilla assistance is insufficient to enhance performance.

3.3. Expressive Model: Cartan Two-Qubit Channels with POVMs

To access the full expressive power of the protocol, we consider a model in which the following applies:

- Each party applies a general two-qubit Cartan (KAK) unitary on the target ⊗ ancilla system;
- The control system is measured using task-dependent two-outcome POVMs.

The resulting strategy is parameterized by 68 real variables. Optimization is performed using the global–local–multi-start pipeline described in Section 2.5.

A preliminary search with limited computational resources yields

$$P_{\text{succ}}^{\text{ext}} \approx 0.6208, \tag{22}$$

indicating strong local basin trapping (Figure 6). Increasing the optimization budget leads to a substantially improved result:

$$P_{\text{succ}}^{\text{ext}} \approx 0.83596, \tag{23}$$

which exceeds the ¾ fixed-order benchmark within the extended protocol and approaches the ideal control-assisted quantum switch value.

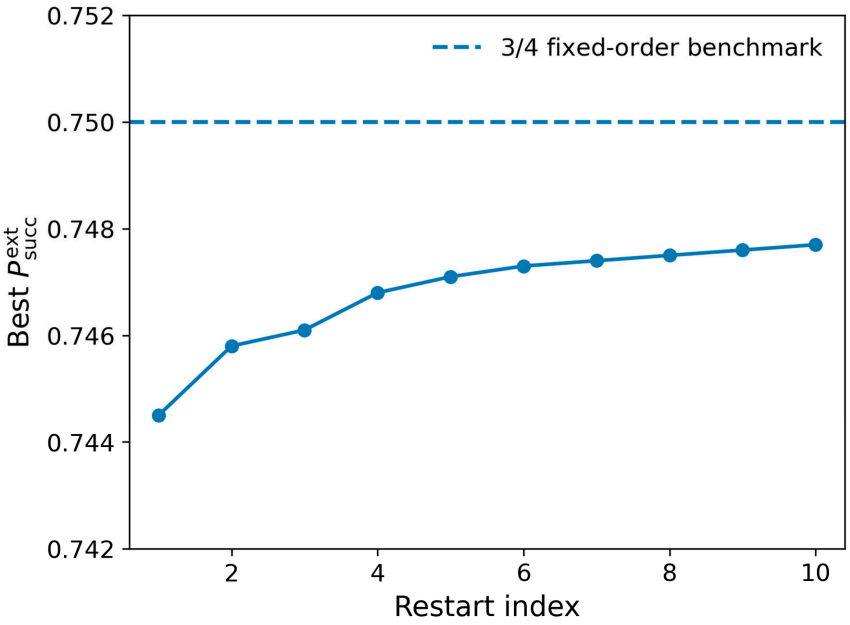


Figure 5. Optimizer performance for the quantum switch with a target–ancilla in the product two-qubit model. Each point shows the best extended success probability $P_{\mathrm{succ}}^{\mathrm{ext}}$ obtained per restart when each party applies a non-entangling product unitary on target $\otimes$ ancilla. The optimizer clusters near $P_{\mathrm{succ}}^{\mathrm{ext}} \approx 0.7477$, again below the $\frac{3}{4}$ fixed-order benchmark, indicating that separable ancilla assistance alone is insufficient to enhance performance within the extended operational protocol.

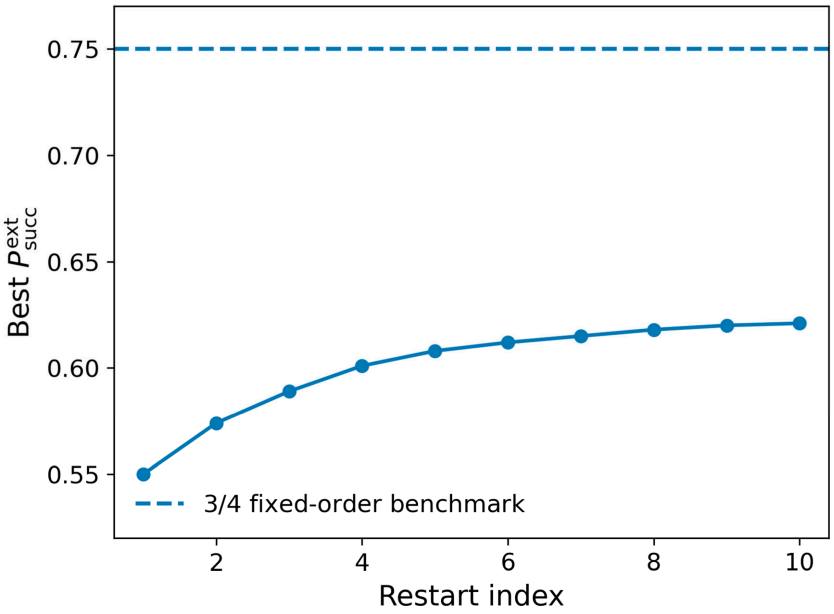


Figure 6. Optimizer performance for the quantum switch with Cartan two-qubit channels and general control POVMs under a lean search budget. Each point shows the best extended success probability $P_{\mathrm{succ}}^{\mathrm{ext}}$ found per restart during an initial compute-limited search over the 68-parameter strategy space. The best value, $P_{\mathrm{succ}}^{\mathrm{ext}} \approx 0.6208$, lies well below the ¾ fixed-order benchmark, illustrating strong local basin trapping under constrained optimization. The solid line connects the best value obtained at each restart to illustrate convergence behavior across optimization runs. It is included for visualization only and has no independent physical significance.

Figure 7 summarizes performance across models, showing that the transition from restricted to fully expressive operations is necessary to achieve an advantage within the extended protocol.

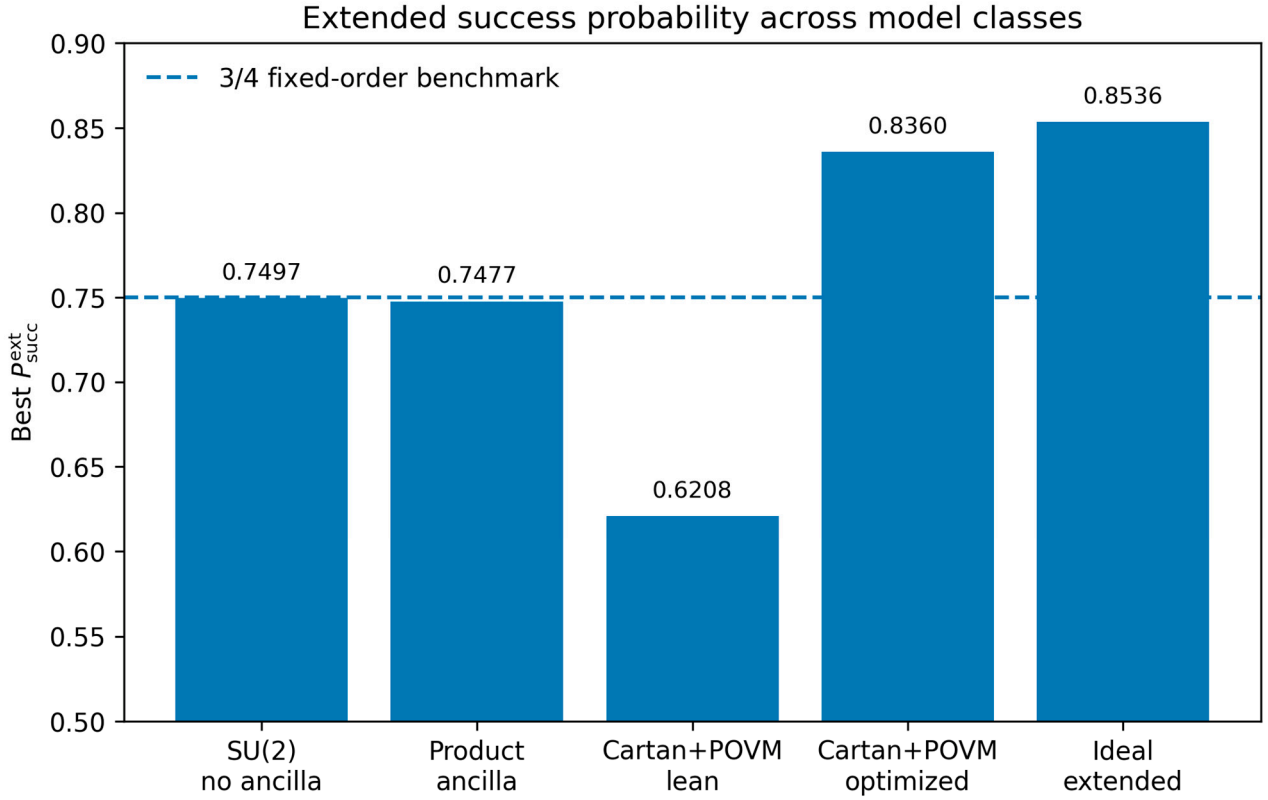


Figure 7. Comparison of best extended success probabilities P_{succ}^{ext} across model classes. Bars show the best value obtained for the SU(2)-only model (no ancilla) and for the optimized Cartan + POVM strategy. The SU(2) model saturates near the ¾ fixed-order benchmark, while the optimized Cartan + POVM model reaches $P_{succ}^{ext} \approx 0.83596$, demonstrating enhanced task performance within the extended operational protocol. The horizontal solid line denotes the reference bound 3/4 used for comparison within the extended operational protocol.

3.4. Operational No-Signaling Verification

We verify operational no-signaling using the conditions defined in Section 2.8. For the optimized parameter set, we compute the conditional distributions and evaluate deviations from perfect independence. The maximum observed deviations are

$$\delta_A \sim 10^{-10}, \delta_B \sim 10^{-10}, \tag{24}$$

which are consistent with numerical precision. This confirms that the enhanced performance is achieved without introducing signaling at the level of observed statistics. We stress that this notion of no-signaling applies to the restricted measurement protocol considered here and does not imply that the underlying process matrix is no-signaling in the general sense.

3.5. Noise Robustness of the Optimized Protocol

We next analyze the robustness of the optimized strategy under white noise. Using the model in Section 2.6, we compute $P_{succ}^{ext}(p)$ for the optimized parameter vector.

The resulting curve (Figure 8) shows that the success probability remains above the 3/4 fixed-order benchmark for noise levels up to approximately

$$p^{\setminus *} \approx 0.256, \tag{25}$$

indicating that the advantage is robust to moderate levels of noise.

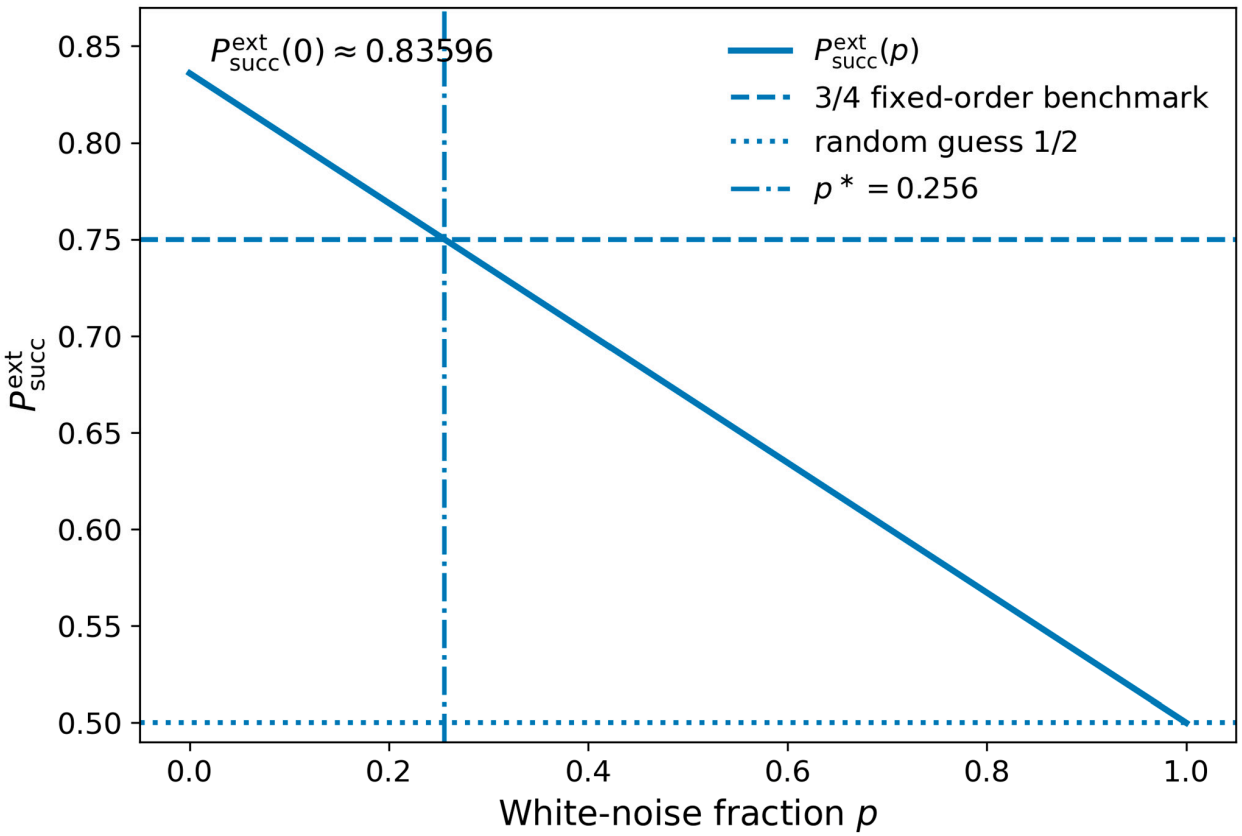


Figure 8. Noise robustness of the optimized Cartan + POVM strategy in the extended operational protocol. The extended success probability $P^{\text{ext}}_{\text{succ}}$ is plotted as a function of white-noise visibility p, obtained by mixing the numerically optimized strategy with a maximally mixed process, as described in Section 2.6. The curve begins at $P^{\text{ext}}_{\text{succ}} \approx 0.83596$ at zero noise and decreases smoothly toward ½ as noise increases, remaining above the ¾ fixed-order benchmark over a finite interval and demonstrating robust enhanced performance. If shown, p^* denotes the critical noise value at which $P^{\text{ext}}_{\text{succ}}$ reaches the ¾ benchmark; the superscript $*$ labels this threshold and is not an independent variable.

3.6. Summary of Results

Table 1 summarizes performance across all models considered. The results demonstrate a clear hierarchy:

- Restricted models (single-qubit and product two-qubit) saturate or remain below the ¾ fixed-order benchmark;
- The fully expressive Cartan + POVM model achieves $P^{\text{ext}}_{\text{succ}} \approx 0.83596$, exceeding the fixed-order benchmark within the extended control-assisted protocol.

Taken together, these findings establish that within the extended operational model defined in Section 2, there exist parameter vectors θ such that

$$P^{\text{ext}}_{\text{succ}}(\theta) > \frac{3}{4}, \tag{26}$$

while satisfying operational no-signaling constraints. This demonstrates a task-level advantage enabled by coherent control of causal order and accessible control system measurements without contradicting known results for causal inequalities in the standard process matrix framework.

Table 1. Summary of success probabilities across model classes in the extended control-assisted protocol.

Condition	Channel/Measurement Family	Best $P_{\text{succ}}^{\text{ext}}$	Fixed-Order Benchmark	Exceeds Benchmark Within Extended Protocol?
Analytic ideal quantum switch	Theoretical control-assisted optimum	0.8536	0.7500	Yes
Simulation: no ancilla	SU(2) per party; projective control measurement	0.7497	0.7500	No
Simulation: with ancilla, product operations	Product SU(2)⊗SU(2) per party; projective control measurement	0.7477	0.7500	No
Simulation: Cartan + POVM, lean search	Entangling two-qubit Cartan operations per party; general control POVMs	0.6208	0.7500	No
Simulation: Cartan + POVM, optimized	Same model, with upgraded global–local–multi-start optimization	0.83596	0.7500	Yes

4. Discussion

The main result of this study is that the quantum switch does not produce enhanced task performance merely because the order of operations is indefinite. In the restricted models, where the parties act with single-qubit SU(2) operations or with non-entangling product operations on a target and ancilla, the optimized success probabilities remain at or below the ¾ fixed-order benchmark. The enhancement appears only in the more expressive Cartan + ancilla + POVM model, where the parties can generate entanglement between target and ancilla and where the control system is measured with sufficient flexibility.

This distinction is important. It shows that the useful resource is not "indefinite order" in isolation. This interpretation is consistent with earlier work treating the order of parties as a quantum resource and with broader analyses of logically consistent and operationally defined quantum causal structures [16–18]. Rather, the advantage comes from a combination of resources: coherent control of the two possible orders, local operations capable of imprinting order-dependent information, and a measurement that can extract this information from the control system. In the optimized model, these ingredients yield $P_{\text{succ}}^{\text{ext}} \approx 0.83596$, which is close to the ideal control-assisted quantum switch value $\left(2+\sqrt{2}\right)/4 \approx 0.8536$.

4.1. Meaning of the Resource Hierarchy

The comparison across model classes gives a useful diagnostic picture. The SU(2)-only model contains the essential feature of the quantum switch: the order of operations is coherently controlled. Nevertheless, this alone is not enough to exceed the fixed-order benchmark. Adding an ancilla also does not help if the operations on target and ancilla remain separable. This suggests that simply enlarging the Hilbert space is not the key ingredient.

The improvement occurs when the model allows for genuinely entangling target–ancilla operations and generalized measurements on the control. The Cartan decomposition

supplies a broad class of two-qubit interactions, while the POVM measurement gives the final readout enough freedom to capture the interference produced by the two alternative orders. This is why the full Cartan + POVM model performs substantially better than the restricted models.

The optimization results also show why this problem is numerically delicate. A lean search in the same expressive model can remain trapped far below the benchmark. The high-performing solution appears only after using a stronger global–local–multi-start search. Thus, the difference between the poor Cartan + POVM search and the optimized Cartan + POVM search should not be interpreted as a change in the underlying physics. It reflects the difficulty of navigating a high-dimensional, non-convex landscape.

4.2. Relation to the Standard LGYNI Result

We therefore compare our results against the standard LGYNI limitation, rather than treating them as a direct violation of that inequality. In the strict process matrix setting, where outputs are generated only by local instruments, quantum theory does not violate the LGYNI causal inequality [13]. The quantum switch is no exception when the future control system is not used as part of the task output.

Experiments with photonic, interferometric, and similar platforms have shown that superpositions of gate orders can be realized in practice [4–7]. Research suggests that indefinite causal order offers benefits for information processing, including improved communication through noisy channels, increased communication capacity, and reduced communication complexity [4,8–12,14].

Prior studies have pointed out some important limitations. Araújo et al. showed that causal non-separability can be confirmed with causal witnesses, but this does not always mean that causal inequalities are violated [3]. Purves and Short found that quantum theory does not break the standard LGYNI causal inequality when only local instruments set the probabilities [13]. More recently, van der Lugt, Barrett, and Chiribella showed that it is possible to certify indefinite causal order in a device-independent way if the scenario includes another spacelike separated observer and Bell-type constraints [15].

The present protocol is therefore not a device-independent violation of the standard LGYNI inequality. It is an extended control-assisted protocol. From this viewpoint, the quantum switch can be understood as a particular higher-order quantum network in which the wiring of operations is itself controlled coherently, rather than fixed in advance [19]. The control system is measured after the switch operation, and that masurement contributes to the output used in the task. For this reason, exceeding ¾ should be described as an extended-protocol task advantage beyond the fixed-order benchmark, not as a standard causal inequality violation.

Figure 9 summarizes the main interpretive distinction of the paper. The same quantum switch idea can appear differently depending on which systems are operationally accessible. If only local instrument statistics are used, the standard LGYNI limitation remains. If the control system is retained and measured as part of an extended task, additional order coherence information becomes available, allowing for performance beyond the fixed-order comparison value.

This point also helps place the work relative to earlier studies. The process matrix framework introduced the possibility of correlations without a predefined causal order [1]. The quantum switch then provided a concrete higher-order transformation in which two operation orders are coherently controlled [2]. Causal witnesses give a device-dependent way to certify causal non-separability [3]. At the same time, causal non-separability is not the same thing as violating a causal inequality. The present work operates in this gap: it does not claim a new device-independent inequality violation but instead analyzes how

control access and measurement structure affect task performance in a concrete quantum switch protocol.

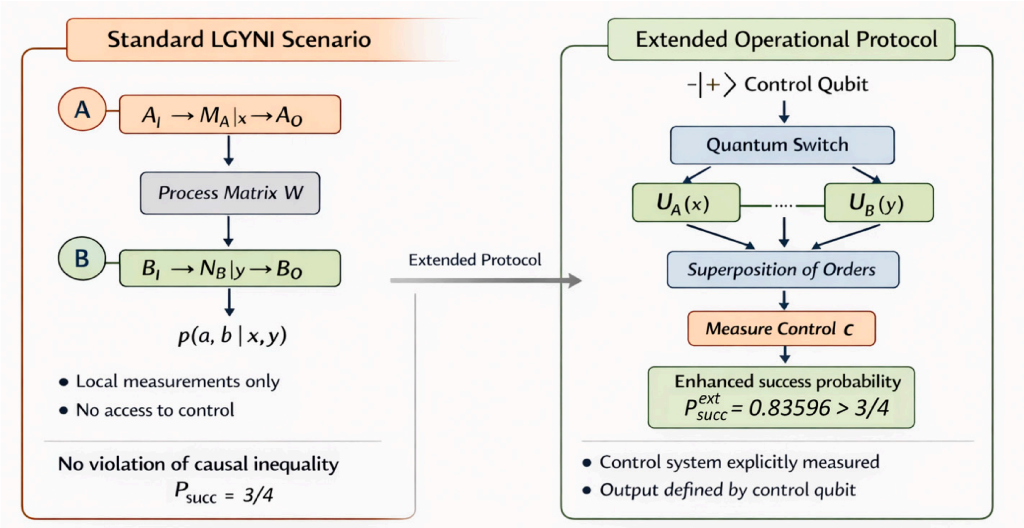


Figure 9. Comparison of causal-game performance in the standard LGYNI scenario and the extended operational protocol considered in this work. Here, A and B denote the two local parties/laboratories in the causal game, with A receiving input x and B receiving input y. In the standard process matrix formulation (**left**), outcomes are generated via local instruments, and the quantum switch does not exceed the LGYNI bound, yielding $P_{\text{succ}} = 3/4$. In the extended protocol (**right**), the control system is explicitly measured and used to define the output variable, leading to enhanced task performance $P^{\text{ext}}_{\text{succ}} \approx 0.83596$. This comparison highlights that the observed enhancement arises from the extended operational setting, rather than from a device-independent violation of the standard LGYNI causal inequality.

4.3. Operational Causality

A vital concern is whether the enhanced performance comes at the cost of causal consistency. However, the no-signaling checks indicate that it does not. For the optimized strategy, the local marginals remain independent of the other party's input to numerical precision. In operational terms, party A's marginal statistics do not depend on y and party B's marginal statistics do not depend on x within the measurement scenario implemented here.

This result is central to the interpretation of the paper. The protocol does not create a channel for signaling to the past, nor does it introduce a causal loop. Instead, it uses interference between the two possible orders as a resource. The order is not fixed in the classical sense, but the observed statistics remain compatible with operational no-signaling.

Thus, our result supports a distinction between temporal order and causal consistency. A definite temporal order is one way to enforce causal consistency, but quantum theory allows for a broader possibility: the order of operations may be coherently controlled while the observable statistics still obey causal constraints.

4.4. Physical and Philosophical Interpretation

The philosophical point requires careful articulation. Our result does not indicate a breakdown of causality; rather, it demonstrates that a process may lack a single definite temporal order while still maintaining causality in the operational sense. Therefore, indefinite causal order should not be conflated with retrocausality, time travel, or closed causal loops.

From a causality-first perspective, the fundamental requirement is that physical processes preserve consistent information flow and avoid causal paradoxes [20–22]. The

quantum switch is compatible with this view. It allows the temporal order of operations to become a quantum degree of freedom, but it does not allow an observer to use that degree of freedom to send information outside of the allowed operational structure.

Our interpretation here is also consistent with chronology protection reasoning [23]. Although the protocol involves a superposition of operation orders, it does not create a closed time-like curve or any usable form of signaling to the past. The nonclassical feature is the coherent organization of alternatives, not a breakdown of causal law.

In this sense, our present results support a moderate interpretation, in that quantum mechanics may relax the requirement of a single classical temporal order while still preserving causality as an operational constraint.

4.5. Hardware Relevance

The protocol is numerical, but it is not disconnected from physical implementation. Quantum switch experiments have already demonstrated coherent superpositions of gate order in photonic and related platforms [4–7]. In such systems, one degree of freedom can serve as the control, while another carries the target state. The present work asks what additional resources would be needed to reproduce the specific task advantage studied here.

For our simulations, we consider the following three requirements for an experimental realization. First, the control degree of freedom must remain coherent long enough for interference between orders to be measured. Second, the target and ancilla must support controllable entangling operations. Third, the final measurement on the control must be flexible enough to implement, or approximate, the optimized POVM.

In photonic systems, these ingredients could be approached using path or polarization control, auxiliary modes, interferometric stability, and generalized measurements implemented through dilation. In circuit-based systems, similar structures might be realized through controlled routing, controlled-SWAP operations, and entangling gates. A full hardware compilation of the optimized Cartan parameters is beyond the scope of this paper, but the resource analysis identifies what such an implementation would require. More broadly, this follows the same resource-oriented logic used in other quantum information settings, where nonclassical physical structure is analyzed for its ability to protect or enhance operational performance [24].

4.6. Relation to Oracle-like Resource Extension

It can be helpful to compare this with oracle models in computation theory, as long as we keep the analogy limited. In an oracle model, a computational system is given access to an additional resource that can change which problems it can solve efficiently [25,26]. In our protocol, access to the control system works in a similar way because it increases the information available for the task by making the order coherence measurable.

However, the control system is not an oracle in the strict sense used in computation theory. It does not provide answers from outside of the physical model. Instead, it is a quantum degree of freedom that holds coherence between the two possible operation orders. The advantage comes when this coherence is kept and turned into useful measurement statistics. So, while the comparison is helpful for understanding, the mechanism is fully physical and follows the usual rules of quantum dynamics [2,8–14].

4.7. Limitations

Several limitations remain. First, the reported enhancement belongs to the extended control-assisted protocol. It should not be described as a device-independent violation of the standard LGYNI causal inequality. The standard no-go result remains valid for the strict local instrument formulation [13].

Second, the present analysis is based on circuit-level simulations. A full device-dependent certification of causal non-separability would require reconstructing or simulating the corresponding process matrix and applying a causal witness SDP [3].

Third, the simulations use idealized unitary operations and idealized measurements. Real hardware will introduce loss, decoherence, imperfect gates, calibration errors, and possibly correlated noise. These effects may change the achievable success probability and the no-signaling deviations. Fourth, the optimization problem is non-convex. The global–local–multi-start procedure finds high-performing strategies, but it does not prove global optimality.

Finally, the conclusions are specific to the task, access assumptions, and model families studied here. Other causal games, other measurement restrictions, or multipartite extensions may lead to different thresholds and resource requirements.

4.8. Summary

Our results show that improved performance in the extended quantum switch protocol requires more than a superposition of orders. The restricted models remain at or below the fixed-order benchmark, whereas the full Cartan + ancilla + POVM strategy exceeds it. This points to entangling dynamics and generalized control measurement as important resources for the observed advantage.

At the same time, the optimized strategy remains operationally no-signaling. The main takeaway is not that causality breaks down but that causal order can act as a quantum resource under carefully defined operational conditions. Even when the order of events is indefinite, causal consistency can remain intact.

5. Conclusions

We have investigated operational causality without definite order by comparing several quantum-switch-based simulation models under the same extended control-assisted task. The results show that coherent control of operation order, by itself, is not sufficient to produce enhanced task performance. Restricted single-qubit SU(2) models and product target–ancilla models remain at or below the $3/4$ fixed-order benchmark. In contrast, the full Cartan + ancilla + POVM model, optimized with a global–local–multi-start pipeline, achieves $P_{\mathrm{succ}}^{\mathrm{ext}} \approx 0.83596$, demonstrating enhanced task performance beyond the fixed-order benchmark within the extended control-assisted protocol.

This result should not be interpreted as a device-independent violation of the standard LGYNI causal inequality. In the strict process matrix formulation, where outcomes are generated only by local instruments, the known no-go result remains valid [13]. The enhancement reported here arises because the protocol retains and measures the control system of the quantum switch, thereby accessing order coherence information that is not available in the standard local instrument setting.

The resource comparison identifies the ingredients required for the enhancement. Ancilla assistance alone is insufficient, and coherent order control alone is insufficient in the restricted models. Enhanced performance appears only when coherent control is combined with entangling target–ancilla dynamics and generalized control system measurements. The optimized strategy also remains operationally no-signaling to numerical precision and is robust to moderate white noise.

These findings support the view that indefinite causal order can be a physically meaningful quantum resource without implying a breakdown of causality. The temporal order of operations may be indefinite, but the observed statistics can still preserve operational causal consistency. In this sense, the results are compatible with a causality-first interpretation: quantum theory may relax the requirement of a single classical temporal order while

still preventing causal paradoxes, retrocausal signaling, or operational time-travel-like behavior [20–23].

The present work provides a reproducible computational framework for studying control-assisted indefinite-order protocols. Future work should focus on full process matrix reconstruction, causal witness certification via semidefinite programming [3], and translation of the optimized Cartan + POVM strategy into experimentally accessible photonic, superconducting, trapped ion, or other quantum information platforms.

Funding: This research received no external funding.

Data Availability Statement: The original contributions presented in this study are included in the article. Further inquiries can be directed to the corresponding author. The simulation code, numerical data, and figure-generation scripts used in this study are available from the corresponding author upon reasonable request. Scripts for the optional SDP-based causal-witness analysis can also be provided upon request.

Acknowledgments: The author gratefully acknowledges administrative and technical support provided during the preparation of this work. The author also acknowledges any in-kind contributions, including materials and related assistance used in the study, where applicable. During the preparation of this manuscript, the author used OpenAI ChatGPT (GPT-5.4 Thinking) for the purposes of language editing, improving clarity and readability, and assisting with drafting and formatting portions of the text. The author reviewed and edited the output and takes full responsibility for the content of this publication.

Conflicts of Interest: The author declares no conflicts of interest.

Appendix A. Mathematical and Computational Details of the Extended Quantum Switch Protocol

This appendix collects the mathematical background and computational implementation details used in the main text. The purpose is to keep the Methods Section 2 readable while providing the explicit process matrix definitions, causal separability structure, quantum switch construction, measurement rules, optimization details, no-signaling checks, and optional causal witness certification.

Appendix A.1. Operational Scenario and Notation

We consider two local laboratories, A and B. Each party receives a classical input bit,

$$x, y \in \{0, 1\},$$

and produces a classical output bit,

$$a, b \in \{0, 1\}.$$

In the process matrix framework, the local operation performed by A, conditioned on input x and output a, is represented by a completely positive map

$$\mathcal{M}^A_{a|x} : \mathcal{L}\left(\mathcal{H}^{A_I}\right) \to \mathcal{L}\left(\mathcal{H}^{A_O}\right), \tag{A1}$$

with Choi operator $M^A_{a|x} \geq 0$. Similarly, party B is described by

$$\mathcal{M}^B_{b|y} : \mathcal{L}\left(\mathcal{H}^{B_I}\right) \to \mathcal{L}\left(\mathcal{H}^{B_O}\right), \tag{A2}$$

with Choi operator $M^B_{b|y} \geq 0$. Complete instruments satisfy the usual normalization conditions corresponding to completely positive trace-preserving maps when summed over outcomes.

A process matrix W is a positive semidefinite operator acting on

$$\mathcal{H}^{A_I} \otimes \mathcal{H}^{A_O} \otimes \mathcal{H}^{B_I} \otimes \mathcal{H}^{B_O}. \tag{A3}$$

It represents the physical process external to the local laboratories. The probabilities generated by local instruments are given by the generalized Born rule,

$$p(a, b \mid x, y) = \mathrm{Tr}\Big[\Big(M^A_{a|x} \otimes M^B_{b|y}\Big) W\Big]. \tag{A4}$$

The process matrix must satisfy positivity and linear normalization constraints so that Equation (A4) gives valid probabilities for all admissible local instruments.

Appendix A.2. Causal Separability and Indefinite Causal Order

A process has definite order $A \prec B$ if A can signal to B, but B cannot signal to A. A process has definite order $B \prec A$ if the reverse condition holds. The corresponding cones of valid fixed-order processes are denoted by

$$\mathcal{W}_{A \prec B} \text{ and } \mathcal{W}_{B \prec A}. \tag{A5}$$

A causally separable process is any convex mixture of fixed-order processes,

$$W_{\text{sep}} = qW_{A \prec B} + (1 - q)W_{B \prec A}, 0 \leq q \leq 1. \tag{A6}$$

Equivalently,

$$\mathcal{W}_{\text{sep}} = \text{conv}(\mathcal{W}_{A \prec B} \cup \mathcal{W}_{B \prec A}). \tag{A7}$$

Such a process may represent classical uncertainty about the order, but each run is still compatible with some definite causal order. A process that cannot be written in the form of Equation (A6) is causally non-separable. This is the process matrix expression of indefinite causal order.

Appendix A.3. Quantum Switch Process Structure

The quantum switch coherently controls the order in which two operations act on a target system. The control qubit is prepared in

$$\mid +\rangle_C = \frac{\mid 0\rangle_C + \mid 1\rangle_C}{\sqrt{2}}. \tag{A8}$$

The branch $\mid 0\rangle_C$ corresponds to one order, and the branch $\mid 1\rangle_C$ corresponds to the reverse order. At the level of process vectors, one may write schematically

$$\mid w_{\text{switch}}\rangle = \frac{1}{\sqrt{2}}(\mid 0\rangle_C \otimes \mid w_{A \prec B}\rangle + \mid 1\rangle_C \otimes \mid w_{B \prec A}\rangle). \tag{A9}$$

The corresponding process matrix is

$$W_{\text{switch}} = \mid w_{\text{switch}}\rangle\langle w_{\text{switch}} \mid . \tag{A10}$$

Expanding Equation (A10) gives

$$W_{\text{switch}} = \tfrac{1}{2}[\ \ |\ 0\rangle\langle 0\ |_C \otimes W_{A\prec B} + |\ 1\rangle\langle 1\ |_C \otimes W_{B\prec A} + |\ 0\rangle\langle 1\ |_C \otimes W_{\text{int}} + |\ 1\rangle\langle 0\ |_C \otimes W_{\text{int}}^{\dagger}]. \tag{A11}$$

The first two terms are the two definite-order branches. The last two terms are coherence, or interference, terms between the two orders. These off-diagonal terms distinguish the quantum switch from a classical random mixture of $A \prec B$ and $B \prec A$.

If the control is traced out or decohered on a $\{|\ 0\rangle, |\ 1\rangle\}$ basis, the interference terms vanish and the process reduces to an incoherent mixture of the two orders. This is why access to the control system is essential in the extended operational protocol studied in this work.

Appendix A.4. Random Task Causal Game and Fixed-Order Benchmark

The task bit $b' \in \{0,1\}$ determines which party must guess the other party's input:

$$b' = 0 : A \text{ must output } a = y,$$
$$b' = 1 : B \text{ must output } b = x.$$

In the standard LGYNI setting, where outputs are generated only by local instruments, the causal inequality benchmark is

$$P_{\text{succ}} \leq \frac{3}{4} \tag{A12}$$

for all causally separable processes.

The intuition is simple. If the order is $A \prec B$, then B can in principle receive information from A, so the branch in which B guesses x can be successful. However, A cannot receive information from B, so the branch in which A guesses y is limited to random guessing. The average is therefore

$$\frac{1}{2}(1) + \frac{1}{2}\left(\frac{1}{2}\right) = \frac{3}{4}. \tag{A13}$$

The same argument applies symmetrically for $B \prec A$, and convex mixtures cannot exceed the same bound.

Appendix A.5. Extended Control-Assisted Success Probability

The present manuscript studies an extended operational protocol. In this protocol, the control system of the quantum switch is measured after the switch operation, and the measurement outcome is used to define the task output.

For uniformly sampled x, y, and b', the extended success probability is

$$P_{\text{succ}}^{\text{ext}}(\theta) = \frac{1}{8}\sum_{x,y\in\{0,1\}} \left[p\left(a = y \mid x, y, b' = 0, \theta\right) + p\left(b = x \mid x, y, b' = 1, \theta\right)\right]. \tag{A14}$$

Here, θ denotes all strategy parameters: local unitary parameters, ancilla couplings, and control measurement parameters.

A value

$$P_{\text{succ}}^{\text{ext}} > \frac{3}{4} \tag{A15}$$

is interpreted as enhanced task performance in the extended control-assisted protocol. It should not be read as a device-independent violation of the standard LGYNI causal inequality, because the output definition now includes access to the control system.

The ideal extended quantum switch construction can reach

$$P_{\text{succ}}^{\text{ext}} = \frac{1}{2}\left(1 + \frac{1}{\sqrt{2}}\right) = \frac{2+\sqrt{2}}{4} \approx 0.853553. \tag{A16}$$

This value depends on preserving coherence between the two orders and measuring the control in a task-dependent basis. If the control is traced out, decohered, or excluded from the output definition, the standard process matrix limitation is recovered.

Appendix A.6. Circuit-Level Quantum Switch Implementation

The simulations use a circuit-level representation of the quantum switch. The control qubit is initialized as in Equation (A8). The target system is initialized in $|\ 0\rangle_t$, and when an ancilla is used it is initialized in $|\ 0\rangle_a$. Thus,

$$|\ \psi_{\text{in}}\rangle = |\ +\rangle_C \otimes |\ 0\rangle_t \tag{A17}$$

for the single-target model, and

$$|\ \psi_{\text{in}}\rangle = |\ +\rangle_C \otimes |\ 0\rangle_t \otimes |\ 0\rangle_a \tag{A18}$$

for the target–ancilla models.

For each input pair (x, y), the switch unitary is

$$U_{\text{switch}}(x,y) = |\ 0\rangle\langle 0\ |_C \otimes U_B(y)U_A(x) + |\ 1\rangle\langle 1\ |_C \otimes U_A(x)U_B(y). \tag{A19}$$

The output state is

$$|\ \psi_{\text{out}}(x,y)\rangle = U_{\text{switch}}(x,y)\,|\ \psi_{\text{in}}\rangle. \tag{A20}$$

This is the state used to evaluate the task-dependent measurement probabilities.

Appendix A.7. SU(2) Parameterization for Restricted Models

In the restricted single-qubit model, each input-dependent operation is a single-qubit unitary parameterized by a ZYZ Euler decomposition,

$$U(\alpha,\beta,\gamma) = e^{-i\alpha Z/2}e^{-i\beta Y/2}e^{-i\gamma Z/2}. \tag{A21}$$

The four unitaries $U_A(0)$, $U_A(1)$, $U_B(0)$, and $U_B(1)$ are each parameterized in this way. This model tests whether coherent control of order and projective control measurement alone are sufficient to exceed the fixed-order benchmark.

In the product target–ancilla model, each party acts on target $\otimes$ ancilla, but only through product operations,

$$U_A(x) = U_A^{(t)}(x) \otimes U_A^{(a)}(x), U_B(y) = U_B^{(t)}(y) \otimes U_B^{(a)}(y). \tag{A22}$$

Each factor is again parameterized by Equation (A21). This model tests whether ancilla assistance without entangling target–ancilla dynamics is sufficient.

Appendix A.8. Projective Control Measurements

In the projective measurement models, the control qubit is measured in a task-dependent basis. For the $b' = 0$ branch, in which A guesses y, the basis is

$$\begin{aligned} \left| \ m_0^{(0)} \right\rangle &= \cos(\phi_0/2) \,|\, 0\rangle + \sin(\phi_0/2) \,|\, 1\rangle, \\ \left| \ m_1^{(0)} \right\rangle &= -\sin(\phi_0/2) \,|\, 0\rangle + \cos(\phi_0/2) \,|\, 1\rangle. \end{aligned} \tag{A23}$$

For the $b' = 1$ branch, in which B guesses x, the basis is

$$\begin{aligned} \left| \ m_0^{(1)} \right\rangle &= \cos(\phi_1/2) \,|\, 0\rangle + \sin(\phi_1/2) \,|\, 1\rangle, \\ \left| \ m_1^{(1)} \right\rangle &= -\sin(\phi_1/2) \,|\, 0\rangle + \cos(\phi_1/2) \,|\, 1\rangle. \end{aligned} \tag{A24}$$

The corresponding projectors are

$$E_{b'}^{(k)} = \left| \ m_k^{(b')} \right\rangle \left\langle m_k^{(b')} \right| . \tag{A25}$$

The correct guess probabilities are

$$p(a = y \mid x, y, b' = 0, \theta) = \langle \psi_{\text{out}}(x, y) \mid \left(E_0^{(y)} \otimes \mathbb{I}_{t,a} \right) \mid \psi_{\text{out}}(x, y) \rangle, \tag{A26}$$

and

$$\mathrm{p(b = x \mid x, y, b' = 1, \theta) = \langle \psi_{out}(x, y) \mid \left(E_1^{(x)} \otimes \mathbb{I}_{t,a} \right) \mid \psi_{out}(x, y) \rangle}. \tag{A27}$$

These are the probabilities inserted into Equation (A14).

Appendix A.9. Cartan/KAK Two-Qubit Parameterization

In the most expressive model, each party applies a general two-qubit unitary on target $\otimes$ ancilla. Each two-qubit block is written using a Cartan, or KAK, decomposition,

$$U = (V_1 \otimes V_2) \exp\left[-\frac{i}{2} (\alpha X \otimes X + \beta Y \otimes Y + \gamma Z \otimes Z) \right] (V_3 \otimes V_4). \tag{A28}$$

Each V_j is a single-qubit SU(2) unitary of the form in Equation (A21), while α, β, and γ are Cartan entangling angles. Thus, each two-qubit block contains 12 local Euler-angle parameters and 3 entangling parameters, for 15 real parameters per block. The full strategy uses $U_A(0)$, $U_A(1)$, $U_B(0)$, and $U_B(1)$, giving 60 channel parameters.

Appendix A.10. General Control POVMs

In the Cartan + POVM model, the projective control measurement is replaced by a two-outcome POVM for each task value b'. The POVM satisfies

$$E_{b'}^{(0)} + E_{b'}^{(1)} = \mathbb{I}_C, E_{b'}^{(k)} \geq 0. \tag{A29}$$

In the implementation, each POVM is represented on a rotated control basis,

$$E_{b'}^{(k)} = V_{b'}^{\dagger} D_{b'}^{(k)} V_{b'}, \tag{A30}$$

where $V_{b'}$ is a control qubit SU(2) rotation. The diagonal entries of $D_{b'}^{(k)}$ are generated from unconstrained real variables using sigmoid maps and normalization. This guarantees positivity and completeness throughout the optimization.

The POVM contributes eight measurement parameters, giving 68 real parameters in the full Cartan + POVM strategy.

Appendix A.11. Numerical Objective and Optimizer Details

The numerical objective is

$$\theta^{\star} = \arg\max_{\theta} P_{\text{succ}}^{\text{ext}}(\theta), \tag{A31}$$

or, equivalently, the minimization of

$$f(\theta) = -P_{\text{succ}}^{\text{ext}}(\theta). \tag{A32}$$

The optimization uses a global–local–multi-start strategy. The global stage uses differential evolution and in higher-budget runs may be supplemented by a covariance matrix adaptation evolution strategy. The best global candidate is then refined using Nelder–Mead. Additional local restarts are launched around the best candidate to reduce the risk of remaining in a shallow local optimum.

All angle-like parameters are restricted to $[-\pi, \pi]$. After noisy perturbations, each angle is wrapped according to

$$\theta_i \mapsto (\theta_i + \pi) \; mod \; (2\pi) - \pi. \tag{A33}$$

Local restart initial points are generated as

$$\theta_0^{(k)} = \theta_{\text{best}} + \sigma\eta^{(k)}, \eta^{(k)} \sim \mathcal{N}(0, \mathbb{I}). \tag{A34}$$

Each perturbed candidate is locally refined. If the refined candidate improves the current value of $P_{\text{succ}}^{\text{ext}}$, the best parameter vector is updated.

Appendix A.12. White Noise Robustness

To quantify robustness, the ideal or optimized success probability is mixed with white noise of strength p. Because a fully noisy strategy gives random guessing, the noisy success probability is modeled as

$$P_{\text{succ}}^{\text{ext}}(p) = (1-p)P_{\text{succ}}^{\text{ext}}(0) + \frac{p}{2}. \tag{A35}$$

The critical noise value $p^\star$ is defined by

$$P_{\text{succ}}^{\text{ext}}(p^\star) = \frac{3}{4}. \tag{A36}$$

Solving Equation (A35) gives

$$p^\star = \frac{P_{\text{succ}}^{\text{ext}}(0) - 3/4}{P_{\text{succ}}^{\text{ext}}(0) - 1/2}. \tag{A37}$$

For the ideal value in Equation (A16), this reduces to

$$p^\star = 2 - \sqrt{2} \approx 0.292893. \tag{A38}$$

For the numerically optimized strategy, Equation (A37) is evaluated using the optimized value of $P_{\text{succ}}^{\text{ext}}(0)$.

Appendix A.13. Operational No-Signaling Checks

Operational causality is verified by checking no-signaling conditions on the observed statistics generated by the implemented protocol. From the joint distribution $p(a, b \mid x, y, b')$, the local marginals are

$$p(a \mid x, y, b') = \sum_b p(a, b \mid x, y, b'), p(b \mid x, y, b') = \sum_a p(a, b \mid x, y, b'). \tag{A39}$$

Operational no-signaling requires

$$p(a \mid x, y, b') \text{ independent of } y, p(b \mid x, y, b') \text{ independent of } x. \tag{A40}$$

The numerical deviations are quantified by

$$\delta_A = \max_{a,x,b'} \mid p(a \mid x, y = 0, b') - p(a \mid x, y = 1, b') \mid, \tag{A41}$$

and

$$\delta_B = \max_{b,y,b'} \mid p(b \mid x = 0, y, b') - p(b \mid x = 1, y, b') \mid . \tag{A42}$$

Values of δ_A and δ_B at numerical precision indicate that the observed statistics are operationally no-signaling for the implemented measurement scenario. This condition is protocol-specific and does not imply that the underlying process matrix is no-signaling in every possible operational context.

Appendix A.14. Causal Witness Certification

A causal witness is a Hermitian operator S that is non-negative on all causally separable processes but negative on at least one causally non-separable process. It satisfies

$$\mathrm{Tr}(SW_{\mathrm{sep}}) \geq 0 \text{ for all } W_{\mathrm{sep}} \in \mathcal{W}_{\mathrm{sep}}, \tag{A43}$$

while, for the process under test,

$$\mathrm{Tr}(SW) < 0. \tag{A44}$$

If such an S exists, then $W \notin \mathcal{W}_{\mathrm{sep}}$, and the process is causally non-separable.

In practice, the witness search is formulated as a semidefinite program over the dual cone of causally separable processes. A convenient form is

$$\begin{array}{ll} \text{minimize} & \mathrm{Tr}(SW) \\ \text{subject to} & \mathrm{Tr}(SW_{A\prec B}) \geq 0 \forall W_{A\prec B} \in \mathcal{W}_{A\prec B}, \\ & \mathrm{Tr}(SW_{B\prec A}) \geq 0 \forall W_{B\prec A} \in \mathcal{W}_{B\prec A}, \\ & \mathrm{Tr}(S\prod_{\mathrm{valid}}) = 1. \end{array} \tag{A45}$$

The last line is a normalization condition used to avoid the trivial zero solution. Equivalent normalizations may also be used. The fixed-order cone constraints are implemented through the standard linear maps enforcing no signaling from future to past for each definite order.

The SDP is implemented in Python/CVXPY, with MOSEK used when available and SCS used for prototyping. This witness analysis is complementary to the extended-protocol success probability analysis. The task success result shows enhanced performance in the extended control-assisted setting; the witness, when reconstructed or simulated process data are available, provides a device-dependent certification of causal non-separability.

Appendix A.15. Interpretation of the 3/4 *Comparison Value*

The value 3/4 is the fixed-order LGYNI benchmark. In the present work, exceeding this value means that the extended control-assisted protocol performs better than the fixed-order benchmark under the stated access assumptions. It does not, by itself, constitute a device-independent violation of the standard LGYNI causal inequality.

The distinction is important. If the control system is inaccessible, traced out, decohered, or excluded from the output definition, the extended-protocol advantage is lost,

and the standard limitation is recovered. The enhancement therefore depends jointly on three ingredients:

1. Coherent control of the two possible orders;
2. Local dynamics capable of imprinting useful order-dependent information;
3. Measurement access to the control system through projective measurements or POVMs.

Appendix A.16. Logical Summary

The logical implications used throughout the manuscript are as follows.

If

$$P_{\text{succ}}^{\text{ext}} \leq \frac{3}{4},$$

then the observed task performance is compatible with the fixed-order benchmark.

If

$$P_{\text{succ}}^{\text{ext}} > \frac{3}{4},$$

then the extended control-assisted protocol shows task-level enhancement beyond the fixed-order benchmark under the stated measurement access assumptions.

If, in addition, a causal witness S satisfies

$$\text{Tr}(SW) < 0,$$

then the reconstructed or simulated process is certified as causally non-separable in a device-dependent sense.

Finally, if the no-signaling deviations δ_A and δ_B are at numerical precision, then the enhanced task performance is achieved without operational signaling in the implemented measurement scenario. Thus, indefinite temporal order does not imply a loss of operational causality.

Appendix B. Protocol Flow Diagrams for the Extended Quantum Switch Simulation

1. Theoretical Framework Setup

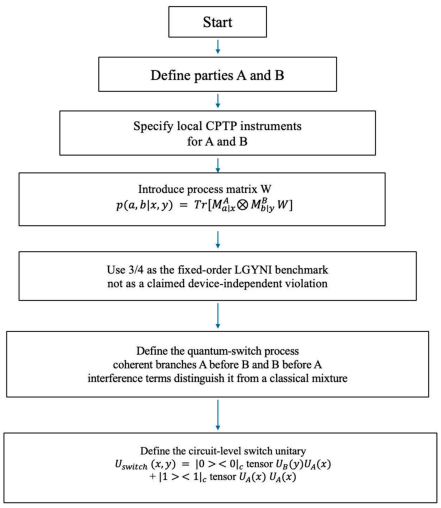


Figure A1. Theoretical setup for the extended quantum switch analysis. The protocol begins by defining the parties A and B, their local CPTP instruments, and the process matrix description. The 3/4 value is used as the fixed-order LGYNI benchmark. The quantum switch is then introduced as a coherent superposition of the two possible orders, with the circuit-level switch unitary providing the simulation model used in the main text.

This diagram illustrates the starting point of the computational protocol used in Section 2.4. The system is prepared in a product state consisting of a superposition over causal orders (via the control qubit) and a fixed initial target/ancilla state. This matches Equation (5) and directly feeds into the construction of the switch unitary.

2. Parameterized Quantum Strategy

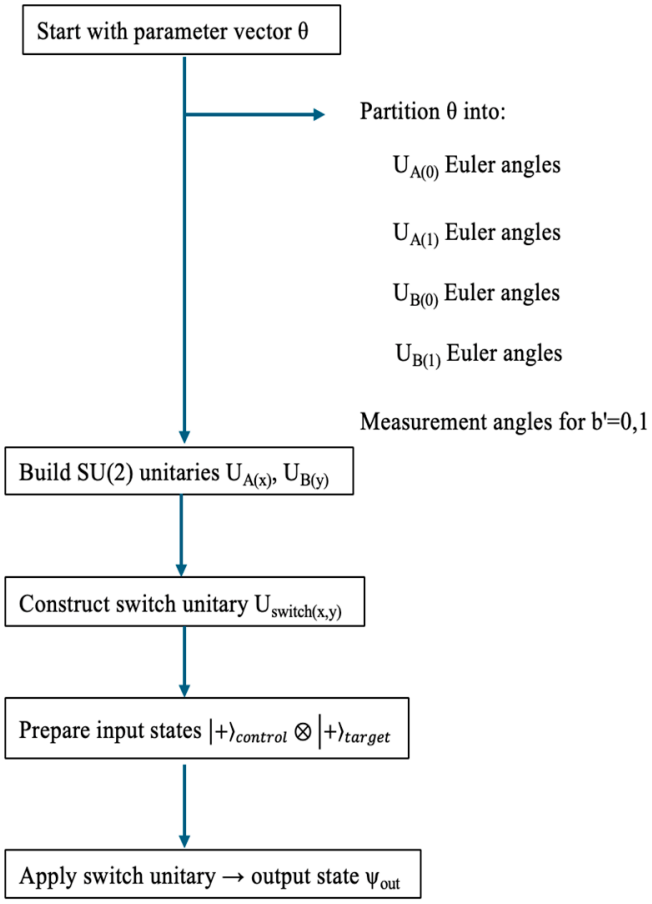


Figure A2. Parameterized quantum strategy used in the extended quantum switch simulation. The parameter vector θ is partitioned into the input-dependent local operations $U_A(0)$, $U_A(1)$, $U_B(0)$, and $U_B(1)$, together with task-dependent control measurement parameters. For each input pair (x, y), the selected operations $U_A(x)$ and $U_B(y)$ are inserted into the quantum switch unitary and applied to the initialized control target state. The resulting state is then passed to the task-dependent measurement stage.

This diagram corresponds to Equation (6) and mirrors the mathematical development in Appendix A, Equations (A9)–(A11). The control-conditioned application of two possible orders lies at the heart of indefinite causal order and is the exact computational representation that the optimizer manipulates.

3. Causal Game Evaluation (Success Probability)

This diagram visualizes Equations (A23) and (A24). It clarifies that the optimization variable ϕ_0 not only defines the measurement axis but directly determines the bias toward correct guessing.

4. Optimization Pipeline

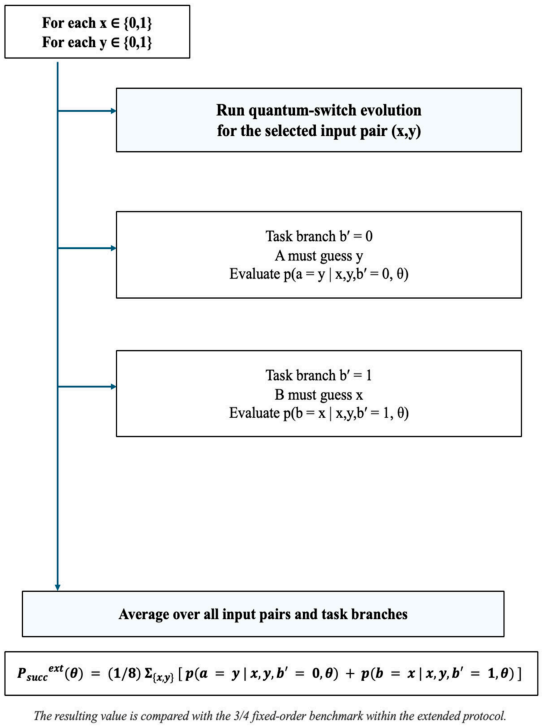


Figure A3. Success probability evaluation in the extended quantum switch protocol. For each pair of inputs x, y, the simulation runs the quantum switch evolution and evaluates both task branches. When $b' = 0$, party A must guess y; when $b' = 1$, party B must guess x. The extended success probability P_{succ}^{ext} is obtained by averaging the correct guess probabilities over all uniformly sampled inputs and task values.

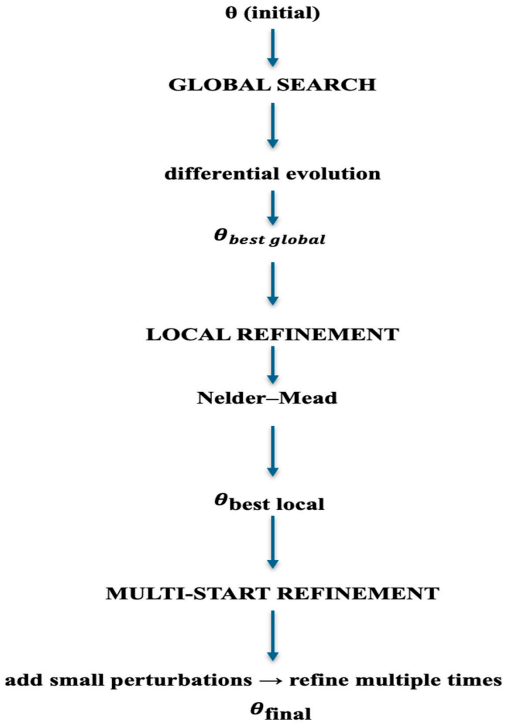


Figure A4. Global–local–multi-start optimization pipeline. Starting from an initial parameter vector θ, the search first uses differential evolution to identify a strong global candidate and then refines that candidate using the Nelder–Mead method. Additional local restarts are performed by perturbing the best parameter vector and refining again. The final output is the optimized parameter vector θ_{final}, which is used to evaluate the best extended-protocol success probability.

This diagram summarizes the numerical search procedure used to obtain the optimized parameter vector reported in the Results. It clarifies that both tasks symmetrically depend on the control channel and the corresponding POVM parameters.

5. Benchmark Comparison for Extended-Protocol Task Advantage

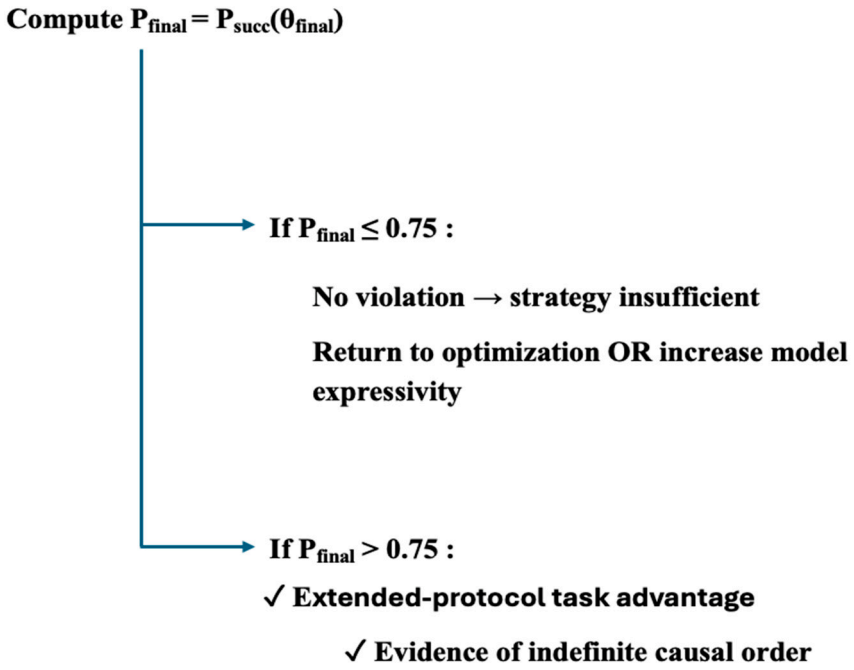


Figure A5. Success probability evaluation and benchmark comparison. For each optimized parameter vector θ, the simulation evaluates the extended success probability $P_{succ}^{ext}(\theta)$ by averaging over all values of x, y, and b′. The optimized value is then compared with the ¾ fixed-order benchmark. Values above this benchmark are interpreted as task-level enhancement within the extended control-assisted protocol, not as device-independent violations of the standard LGYNI causal inequality.

This diagram represents Equation (4). It shows how the optimizer ultimately evaluates the objective function used in the global–local–multi-start pipeline described in Section 2.7.

6. Optional Causal Witness Certification

Causal Witness Certification Pipeline. The diagram in Figure A6 summarizes the optional formal certification stage implemented after obtaining an optimized strategy $\theta^{\setminus *}$. While the main text bases causal non-separability on the extended-protocol task success analysis $P_{succ}^{ext}\left(\theta^{\setminus *}\right) > 3/4$, the process matrix formalism also allows for a *device-dependent* certificate known as a causal witness [3].

To construct such a witness, one first reconstructs or simulates the process matrix $W\left(\theta^{\setminus *}\right)$ associated with the optimized strategy. Then a semidefinite program searches for an operator S satisfying the following:

1. $\mathrm{Tr}\left(SW_{\mathrm{sep}}\right) \geq 0$ for all causally separable processes W_{sep} (dual-cone constraint);
2. $\mathrm{Tr}\left(SW\left(\theta^{\setminus *}\right)\right) < 0$ (non-separability detected);
3. A normalization constraint, such as $\mathrm{Tr}(S\prod_{\mathrm{valid}}) = 1$.

If such an S exists, the optimized process is provably causally non-separable. Because witness certification is more computationally expensive and requires process reconstruction, we present it as an optional but powerful extension.

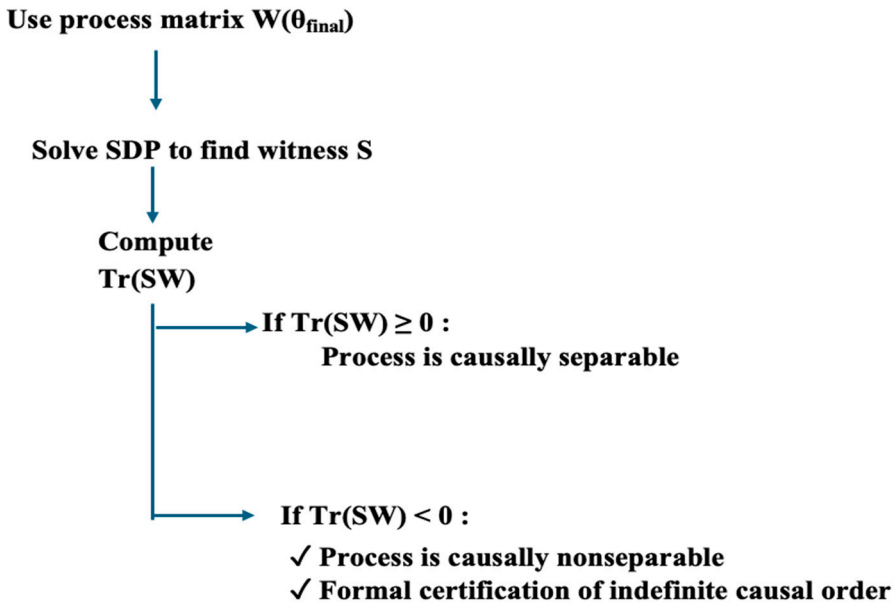


Figure A6. Optional causal witness certification pipeline. After an optimized strategy $\theta^{\star}$ is obtained, one may simulate or reconstruct the associated process matrix $W(\theta^{\star})$. A semidefinite program then searches for a causal witness S. If $\mathrm{Tr}(SW) < 0$, the reconstructed or simulated process is certified as causally non-separable in a device-dependent sense. This step is complementary to the extended-protocol task success analysis and is not required to compute $P_{\mathrm{succ}}^{\mathrm{ext}}$.

References

1. Oreshkov, O.; Costa, F.; Brukner, Č. Quantum correlations with no causal order. *Nat. Commun.* **2012**, *3*, 1092. [CrossRef] [PubMed]
2. Chiribella, G.; D'Ariano, G.M.; Perinotti, P.; Valiron, B. Quantum computations without definite causal order. *Phys. Rev. A* **2013**, *88*, 022318. [CrossRef]
3. Araújo, M.; Branciard, C.; Costa, F.; Feix, A.; Giarmatzi, C.; Brukner, Č. Witnessing causal nonseparability. *New J. Phys.* **2015**, *17*, 102001. [CrossRef]
4. Procopio, L.M.; Moqanaki, A.; Araújo, M.; Costa, F.; Calafell, I.A.; Dowd, E.G.; Hamel, D.R.; Rozema, L.A.; Brukner, Č.; Walther, P. Experimental superposition of orders of quantum gates. *Nat. Commun.* **2015**, *6*, 7913. [CrossRef]
5. Rubino, G.; Rozema, L.; Feix, A.; Araújo, M.; Zeuner, J.M.; Procopio, L.M.; Brukner, C.; Walther, P. Experimental verification of an indefinite causal order. *Sci. Adv.* **2017**, *3*, e1602589. [CrossRef]
6. Wei, K.; Tischler, N.; Zhao, S.R.; Li, Y.H.; Arrazola, J.M.; Liu, Y.; Zhang, W.; Li, H.; You, L.; Wang, Z.; et al. Experimental quantum switching for exponentially superior quantum communication complexity. *Phys. Rev. Lett.* **2019**, *122*, 120504. [CrossRef] [PubMed]
7. Goswami, K.; Giarmatzi, C.; Kewming, M.J.; Costa, F.; Branciard, C.; Romero, J.; White, A.G. Indefinite causal order in a quantum switch. *Phys. Rev. Lett.* **2018**, *121*, 090503. [CrossRef]
8. Ebler, D.; Salek, S.; Chiribella, G. Enhanced communication with the assistance of indefinite causal order. *Phys. Rev. Lett.* **2018**, *120*, 120502. [CrossRef]
9. Abbott, A.A.; Wechs, J.; Horsman, D.; Mhalla, M.; Branciard, C. Communication through coherent control of quantum channels. *Quantum* **2020**, *4*, 333. [CrossRef]
10. Goswami, K.; Cao, Y.; Paz-Silva, G.A.; Romero, J.; White, A.G. Communicating via ignorance: Increasing communication capacity via superposition of order. *Phys. Rev. Res.* **2020**, *2*, 033292. [CrossRef]
11. Guérin, P.A.; Feix, A.; Brukner, Č. Exponential communication complexity advantage from quantum superposition of the direction of communication. *Phys. Rev. Lett.* **2016**, *117*, 100502. [CrossRef]
12. Procopio, L.M.; Delgado, F.; Enríquez, M.; Belabas, N.; Levenson, J.A. Communication Enhancement Through Quantum Coherent Control of *N* Channels in an Indefinite Causal-Order Scenario. *Entropy* **2019**, *21*, 1012. [CrossRef]
13. Purves, T.; Short, A.J. Quantum theory cannot violate a causal inequality. *Phys. Rev. Lett.* **2021**, *127*, 110402. [CrossRef]
14. Colnaghi, T.; D'Ariano, G.M.; Facchini, S.; Perinotti, P. Quantum computation with programmable connections between gates. *Phys. Lett. A* **2012**, *376*, 2940–2943. [CrossRef]
15. Van Der Lugt, T.; Barrett, J.; Chiribella, G. Device-independent certification of indefinite causal order in the quantum switch. *Nat. Commun.* **2023**, *14*, 5811. [CrossRef] [PubMed]
16. Feix, A.; Brukner, Č. Quantum superpositions of the order of parties as a resource. *Phys. Rev. A* **2015**, *92*, 052326. [CrossRef]

17. Baumeler, Ä.; Wolf, S. The space of logically consistent classical processes without causal order. *New J. Phys.* **2016**, *18*, 013036. [CrossRef]
18. Wechs, J.; Abbott, A.A.; Costa, F.; Branciard, C. On the definition of quantum causality. *Quantum* **2019**, *3*, 150.
19. Chiribella, G.; D'Ariano, G.M.; Perinotti, P. Theoretical framework for quantum networks. *Phys. Rev. A* **2009**, *80*, 022339. [CrossRef]
20. Crogman, H.; Jackson, M.; Peters, R. A causality framework reflecting and contextualizing physical reality in terms of the presentist's conception of our universe. *Phys. Essays* **2017**, *30*, 200–223. [CrossRef]
21. Brukner, Č. Quantum causality. *Nat. Phys.* **2014**, *10*, 259–263. [CrossRef]
22. Hardy, L. Operational generalized probability theory, composition, and causality. *Philos. Trans. R. Soc. A* **2016**, *374*, 20150248.
23. Hawking, S.W. Chronology protection conjecture. *Phys. Rev. D* **1992**, *46*, 603. [CrossRef] [PubMed]
24. Crogman, H.T.; Dang, T.; Erenso, D. Topologically Protected Quantum Teleportation via Majorana Zero Modes: A Perspective on Scalability and Decoherence Immunity. *Quantum Rep.* **2025**, *7*, 42. [CrossRef]
25. Turing, A.M. Systems of Logic Based on Ordinals. *Proc. Lond. Math. Soc.* **1939**, *s2-45*, 161–228. [CrossRef]
26. Bennett, C.H.; Bernstein, E.; Brassard, G.; Vazirani, U. Strengths and Weaknesses of Quantum Computing. *SIAM J. Comput.* **1997**, *26*, 1510–1523. [CrossRef]

Disclaimer/Publisher's Note: The statements, opinions and data contained in all publications are solely those of the individual author(s) and contributor(s) and not of MDPI and/or the editor(s). MDPI and/or the editor(s) disclaim responsibility for any injury to people or property resulting from any ideas, methods, instructions or products referred to in the content.